



RESEARCH ARTICLE

10.1029/2021JD035025

Key Points:

- A model experiment is used to test the impact of the Hoggar mountains on dust emission frequency in the Sahara
- The mountains generate a leeward low due to elevated heating
- Removing the mountains reduces emission frequency in the highly active Tidihelt by 31%

Correspondence to:





T. Caton Harrison,
thoton@bas.ac.uk

Citation:

Caton Harrison, T., Washington, R., Engelstaedter, S., Jones, R. G., & Savage, N. H. (2021). Influence of orography upon summertime low-level jet dust emission in the central and western Sahara. *Journal of Geophysical Research: Atmospheres*, 126, e2021JD035025. <https://doi.org/10.1029/2021JD035025>

Received 7 APR 2021
Accepted 27 OCT 2021

Influence of Orography Upon Summertime Low-Level Jet Dust Emission in the Central and Western Sahara

Thomas Caton Harrison^{1,2} , Richard Washington¹, Sebastian Engelstaedter¹ ,
Richard G. Jones^{1,3} , and Nick H. Savage³ 

¹Climate Research Laboratory, Oxford University Centre for the Environment, Oxford, UK, ²British Antarctic Survey, Cambridge, UK, ³Met Office, Exeter, UK

Abstract Low-level jets (LLJs) drive frequent emission of mineral dust in the central and western Sahara in boreal summer. A major hotspot for this process is central Algeria, northern Mali and Mauritania, through which blow the dry near-surface northeasterly Harmattan winds, with a peak in dust emission around the low-lying Tidihelt region. North African orography is thought to contribute to the strength of the LLJ over the Bodele dust source in Chad, but its influence on erosivity over summertime source regions remains unquantified. In this paper, the contribution of central Saharan orography to the strength of Harmattan LLJs and associated dust emission frequency is tested. An idealized simulation with flattened Hoggar mountains is compared with a control using the Met Office Unified Model at 12 km horizontal resolution. In the absence of the Hoggar mountains, dust emission frequency estimated using an empirical relationship with surface wind speeds is found to decline across the entire northeasterly “LLJ alley,” including by 31% in the Tidihelt where composited jet surface winds drop from 9.0 to 7.3 m s⁻¹ under a more easterly regime. The mountains are linked to a low-level leeward geopotential height perturbation, with a northern limb reinforcing northeasterlies through the Tidihelt. Dome-shaped elevated heating situated over the Hoggar mountains explains the difference between the simulated wind fields in the two experiments. These findings suggest that central Saharan orography plays an important role in sustaining erosive dusty conditions during boreal summer.

Plain Language Summary A major driver of dust storms in the central and western Sahara is a strong wind (referred to as a jet) which forms overnight at elevation and then hits the surface after sunrise. This process is important in the remote central Algerian Tidihelt region, home to a highly active dust source. In this paper we estimate the effect that the nearby Hoggar mountains have upon strong wind events in the Tidihelt during summer. We do this by comparing two computer model simulations of the atmosphere over North Africa. One has a realistic representation of the Hoggar mountains, whereas in the other the mountains are flattened to a uniform level. Our results show that the mountains strengthen these winds by heating the atmosphere relative to the surrounding desert, producing a local region of low pressure. Using satellite observations of dust plumes we estimate that without the mountains the frequency of dust emission events from the Tidihelt would be reduced by about a third due to weaker winds. The findings show how mountains can play an important role in the meteorology responsible for dust storms.

1. Introduction

1.1. Background

Mineral dust is an abundant and important aerosol with natural and anthropogenic origins. The largest proportion of atmospheric loading of mineral dust originates from the Sahara, with peak emission in boreal spring and summer (Kok et al., 2021). Saharan dust has a varied radiative effect (Boucher et al., 2013), as well as impacts on ice nucleation (Hoose et al., 2008), tropical cyclone development (Strong et al., 2018), rainforest fertilization (Mahowald et al., 2010), ocean biogeochemistry (Jickells et al., 2005; Schulz et al., 2012) and human health (De Longueville et al., 2010). Activation of Saharan dust sources is sporadic and sensitive to relatively infrequent intense winds linked to mesoscale atmospheric processes (Allen et al., 2013; Caton Harrison et al., 2019; Cowie et al., 2015; Marsham et al., 2013).

Dust models diverge considerably in their estimates of net North African yearly dust fluxes (Huneeus et al., 2011; Wu et al., 2020). Although part of this is due to the formulation of the model itself, a large proportion of the uncertainty stems from differences between driving wind fields (Fiedler et al., 2016; Luo et al., 2003). To address

© 2021. The Authors.

This is an open access article under the terms of the [Creative Commons Attribution License](https://creativecommons.org/licenses/by/4.0/), which permits use, distribution and reproduction in any medium, provided the original work is properly cited.

these sources of uncertainty, several modeling and observation studies have attempted to characterize the mesoscale processes responsible for dust emission (e.g., Allen et al., 2013; Caton Harrison et al., 2019, 2021; Heinold et al., 2013; Knippertz et al., 2007; Schepanski et al., 2009; Washington & Todd, 2005; Washington et al., 2006) and to evaluate their representation in wind speed products commonly used to drive offline dust models (Allen & Washington, 2014; Garcia-Carreras et al., 2013; Roberts et al., 2017; Schepanski et al., 2015).

A major meteorological emission mechanism at work in the Sahara during boreal summer is the morning breakdown of the nocturnal low-level jet (LLJ). Winds atop the nocturnal boundary layer accelerate under a stable regime due to decoupling from surface friction and inertial oscillation (Blackadar, 1957). Mixing of jet momentum to the surface as a result of eddy-driven turbulence in the morning raises surface wind speeds, leading to dust emission in the strongest cases (Allen & Washington, 2014). An analysis of the ERA-Interim reanalysis indicates that favorable locations for LLJs are found along the margins of the Saharan heat low (SHL) in regions of Atlantic, Mediterranean and monsoon inflow, as well as downwind of orographic channels (Fiedler et al., 2013). LLJs embedded in both northeasterly and monsoon flows were regularly observed during the June 2011 intensive observation period of the Fennec campaign, contributing 14% of the observed dust loading (Allen & Washington, 2014; Allen et al., 2013). Automated tracking of over 47,000 summertime dust plumes observed in SEVIRI from 2004 to 2017 indicates that LLJs are responsible for 18% of flagged dust pixels, and as much as 40% in 2012 (Caton Harrison et al., 2019).

A robust feature of both model and satellite analyses of Saharan dust is a prominent hotspot of dust presence and emission around central Algeria (Ashpole & Washington, 2013; Evan et al., 2015; Heinold et al., 2013; Schepanski et al., 2007; Todd & Cavazos-Guerra, 2016; Wu et al., 2020), as well as more generally within the broad northeasterly Harmattan 'alley' of the northern Sahara. The central Algerian surface wind speed maximum, referred to as the Tidihelt jet in this paper, is evident in reanalysis (see e.g., Figure 13g–13i in Caton Harrison et al. [2019]) and surface observations (Chellali et al., 2011; Messaoudi et al., 2019). The Tidihelt region is unique in that unlike almost all other dust sources, it is predominantly activated by LLJs (Caton Harrison et al., 2019). A map of the Tidihelt dust source showing potential erodible salt flats is given in Figure 15 of Caton Harrison et al. (2019). The LLJ alley containing the Tidihelt jet is bounded by the Atlas mountains to the north and the Hoggar mountains to the south (see Figure 3a).

1.2. Orographic Effects on Dust-Emitting Conditions in the Sahara

Although the proximity of many Saharan dust sources to orographic channels has been noted (Evan et al., 2015; Fiedler et al., 2013; Schepanski et al., 2007), few studies have drawn an explicit link between Saharan orography and the frequency or strength of dust emission, especially for western sources such as the Tidihelt. The Bodele in northern Chad is frequently activated when a ridging Libyan high pressure system drives statically stable northeasterlies through a gap between the Tibesti and Ennedi massifs, splitting the flow upstream and accelerating winds in the exit region by up to 40% (Todd et al., 2008; Washington et al., 2006). A secondary effect from elevated heating and cooling over the mountains is also apparent. The Bodele is much larger and more active than western Saharan dust sources, but serves nonetheless as a useful analogue.

Western Saharan orography stretching from the Atlas mountains in the north to the Air mountains in the south has been linked to atmospheric phenomena relevant to dust emission. Kelvin waves regularly propagate along the barrier of the Atlas mountains, organizing downslope winds and jet adjustment processes responsible for severe dust storms in the Harmattan channel (Pokharel & Kaplan, 2019). A relationship may also exist between the Atlas range and the remote Saharan boundary layer, with ascent over the mountains and compensating descent over the central Sahara (Flamant et al., 2007). There is also a plausible but untested connection between orography and triggering of convection in the southern Sahara during the late monsoon season, which in turn produces convective downdrafts responsible for dust emission (Caton Harrison et al., 2021).

The Hoggar mountains south of the Tidihelt have a peak of 2,918 m, span 800 km and consist of rock pinnacles and volcanogenic formations, with widespread dust sources in their western lee and southern flank formed from outwash fluvial and paleo-lacustrine deposits (Ashpole & Washington, 2013; Prospero et al., 2002). These mountains are thought to have some role in the onset of the West African Monsoon due to their interaction with the SHL via lee cyclogenesis. It has been shown that background easterlies and northeasterlies around the mountains could be capable of initiating a leeward trough or depression as the subtropical anticyclone is amplified over the

elevated terrain, in turn deepening the SHL (Drobinski et al., 2005; Semazzi & Sun, 1997). The mechanics of such a process have not been demonstrated in detail, however, and have not been linked directly to dust emission. Birch et al. (2012) previously flattened the Hoggar mountains in a set of idealized model experiments using the Met Office Unified Model, showing how orography heats and deepens the convective boundary layer over the Sahara several hundred kilometers west of the main peaks, and redirects cooler maritime easterlies upstream. These thermodynamic effects could offer an additional or alternative explanation for the interaction between the Hoggar mountains and summertime dust emission, but the effect of orography upon dust emission frequency from nearby dust sources has not been explored.

1.3. Aims

In this paper, we test the effect of the Hoggar mountains upon a prominent climatological peak in summertime wind speeds over central Algeria associated with a frequent LLJ, identified here as the Tidihelt jet. Boreal summer is selected for analysis as dust emission from the central and western Sahara, including central Algeria, is high at this time of year (Engelstaedter et al., 2006; Kok et al., 2021; Ridley et al., 2012; Schepanski et al., 2012) and because automated satellite detection of LLJ has been developed for the summer months (Caton Harrison et al., 2019). The study also estimates the impact of these winds on dust emission frequency. To achieve this, we identify the synoptic conditions favoring the Tidihelt jet, test for elevated heating and lee cyclogenesis associated with the elevated terrain and estimate the wider impacts of the orography upon dust emission frequency in the northern Saharan LLJ alley. In summary, the research aims to:

1. Quantify the effect of the Hoggar mountains upon dust-emitting winds in central Algeria
2. Identify a mechanism linking the Hoggar mountains and elevated surface wind speeds
3. Estimate the effect of the Hoggar mountains upon dust emission frequency within the LLJ alley of the northern Sahara

Model and observation datasets are described in Section 2, as well as a composite method. The synoptic conditions associated with dust emission in central Algeria are described in Section 3, with the results of the model experiment presented in Section 4.

2. Data and Model Experiment Setup

2.1. Model Data

This study uses a regional climate model (HadREM3-GA7.05) in a limited area configuration of the GA7.05 Unified Model (UM) (Walters et al., 2019), closely based on the model configuration used in UKCP18 climate projections (Murphy et al., 2018). It is set up in atmosphere-only mode with a limited area domain centered over North Africa on a 12 km horizontal grid with 57 vertical levels. The UM dynamical core solves deep-atmosphere non-hydrostatic equations with a semi-implicit, semi-Lagrangian formulation discretized onto a regular latitude-longitude grid with terrain-following hybrid height coordinates (Walters et al., 2019). In this configuration, convection is parameterized and sea surface temperatures and sea ice extents are prescribed using the analyses of Reynolds et al. (2002), in addition to aerosol properties and cloud droplet number concentration derived from the MACv2-SP dataset for the historical (Stevens et al., 2017) scenario. The method used to implement these aerosol effects is identical to that used in the 12 km RCM in UKCP, although with a difference source dataset. As dust emission is not explicitly simulated, the effects of winds upon dust emission are derived empirically based on satellite-observed dust source LLJ activity, described in Section 2.2.

Of particular relevance to the simulation of LLJs is the boundary layer scheme. While inertial oscillation is handled by the dynamical core, the UM boundary layer scheme (Brown et al., 2008; Lock et al., 2000) is responsible for all vertical mixing by turbulent motions and is therefore critical for LLJ decoupling and decay. In an unstable boundary layer, diffusion coefficients (K profiles) are defined for sources of turbulence from both the surface and cloud top, whereas in a stable regime a local Richardson number scheme (Smith, 1990) applies. Shallow and deep sub-grid cumulus convection is handled by the UM mass-flux convection scheme, with an extension to include parameterization of downdrafts (Gregory & Rowntree, 1990; Walters et al., 2019).

Lateral boundary conditions and initial conditions are supplied to the limited area model by the ERA-Interim reanalysis (Dee et al., 2011) via one-way nesting. ERA-Interim has a horizontal resolution of approximately 80 km, and helps align the model with the quasi-observed state of the atmosphere represented in the reanalysis as it steps forwards in time, although the region of interest is far away from the domain boundaries at 20.1°W to 23.8°E and 7.9°N to 37.6°N meaning the UM plays a dominant role in the simulation of LLJ processes therein. Output is analyzed from June, July, and August 2004 to 2007, but simulations are run from May 2004 to August 2007 to allow for one month of model spin-up. Although ERA-Interim underestimates surface winds associated with Saharan LLJs (Allen & Washington, 2014), it is capable of realistically reproducing wind variability associated with synoptic and seasonal variations (Roberts et al., 2017) which is important for lateral boundary conditions.

2.2. Observations

A key characteristic of the summertime Sahara is that the majority of dust sources, including many in the Harmattan channel, are regularly influenced by cold pool outflows (CPOs) (Caton Harrison et al., 2019). In this paper, data from the Spinning Enhanced Visible and Infrared Imager (SEVIRI) are used to identify days with dust present and to compare simulated wind speeds with dust emission frequency. Dust is identified in SEVIRI from Brightness Temperatures at 15 min intervals and 3 km nadir resolution using the SEVIRI dust flags approach of Ashpole and Washington (2012) and subsequently filtered to identify plumes associated with LLJ activity following the method in Caton Harrison et al. (2019). Critically, this allows dust associated with LLJs to be distinguished from CPO dust. Although SEVIRI is commonly used for dust detection (Ackerman, 1997; Lensky & Rosenfeld, 2008; Schepanski et al., 2007), split-window techniques using wavelengths from 8 to 12 μm such as SEVIRI dust flags are also sensitive to column water vapor and cloud (Brindley et al., 2012). Central Algeria is partly spared from such drawbacks as it is exceptionally dry and has a high percentage of cloud-free days (e.g., see Figure 13 in Caton Harrison et al. [2019]).

Radiosonde data used in this paper to identify synoptic conditions linked to dust emission are obtained for In Salah (27.19°N, 2.47°E), approximately 150 km upwind (northeast) of the Tidihelt dust sources. Daily soundings at 12:00 UTC are sourced from the Integrated Global Radiosonde Archive (Durre et al., 2006) maintained by the National Centers for Environmental Information.

2.3. Model Validation

The UM is selected as the modeling system for this project as it has demonstrable fidelity in simulating both the large-scale synoptics and the jet core wind speeds within the boundary layer. A 12 km horizontal grid-spacing configuration of the UM has been deployed (as 'Africa-LAM') to support the Fennec Campaign of in-situ observations in 2011 and 2012 (Washington et al., 2012). Comparisons between Africa-LAM and observations from supersite 1 located at Bordj-Badji Mokhtar in southern Algeria (approximately 500 km south of the Tidihelt region defined in Section 2.5) reveal 'excellent agreement' between model wind speed profiles at 06:00 UTC and Lidar measurements for Harmattan LLJs (Allen & Washington, 2014), equivalent to the northeasterly jets considered in this paper. Allen et al. (2015) also find a hit rate of 85% in simulating morning LLJ winds at the surface compared to Fennec automatic weather station data, but they note that the frequency of the highest ($>10 \text{ m s}^{-1}$) winds is underestimated. Dropsonde measurements from Fennec flights show that forecasts accurately represent large-scale wind fields around the SHL but underestimate morning wind speeds (Engelstaedter et al., 2015).

Figure 1 compares the 12 km configuration of the UM used in this paper with the approximately 31 km resolution ERA5 reanalysis. With a severe paucity of in-situ observations in the central Sahara, there is little for reanalyses to assimilate and dust extinction is not generally included in temperature or humidity retrievals from satellite infrared sensors, leading to biases in these assimilated variables (Weaver et al., 2003). As a result, significant disagreements exist between reanalyses over North Africa. This has led to uncertainty in their ability to faithfully represent the SHL (Marshall et al., 2011), mesoscale convective systems (Roberts & Knippertz, 2014) and the intertropical discontinuity (Roberts et al., 2015). Comparison against ground stations from other parts of the world indicates ERA5 outperforms other reanalyses in representing diurnal variability of surface winds (Ramon et al., 2019), but an extensive evaluation of ERA5 winds against ground stations and other reanalyses has not yet been carried out over the Sahara. We adopt it here only for a broad comparison of synoptic features, given that it likely inherits underestimation of peak Saharan surface winds shown in ERA-Interim (Allen &

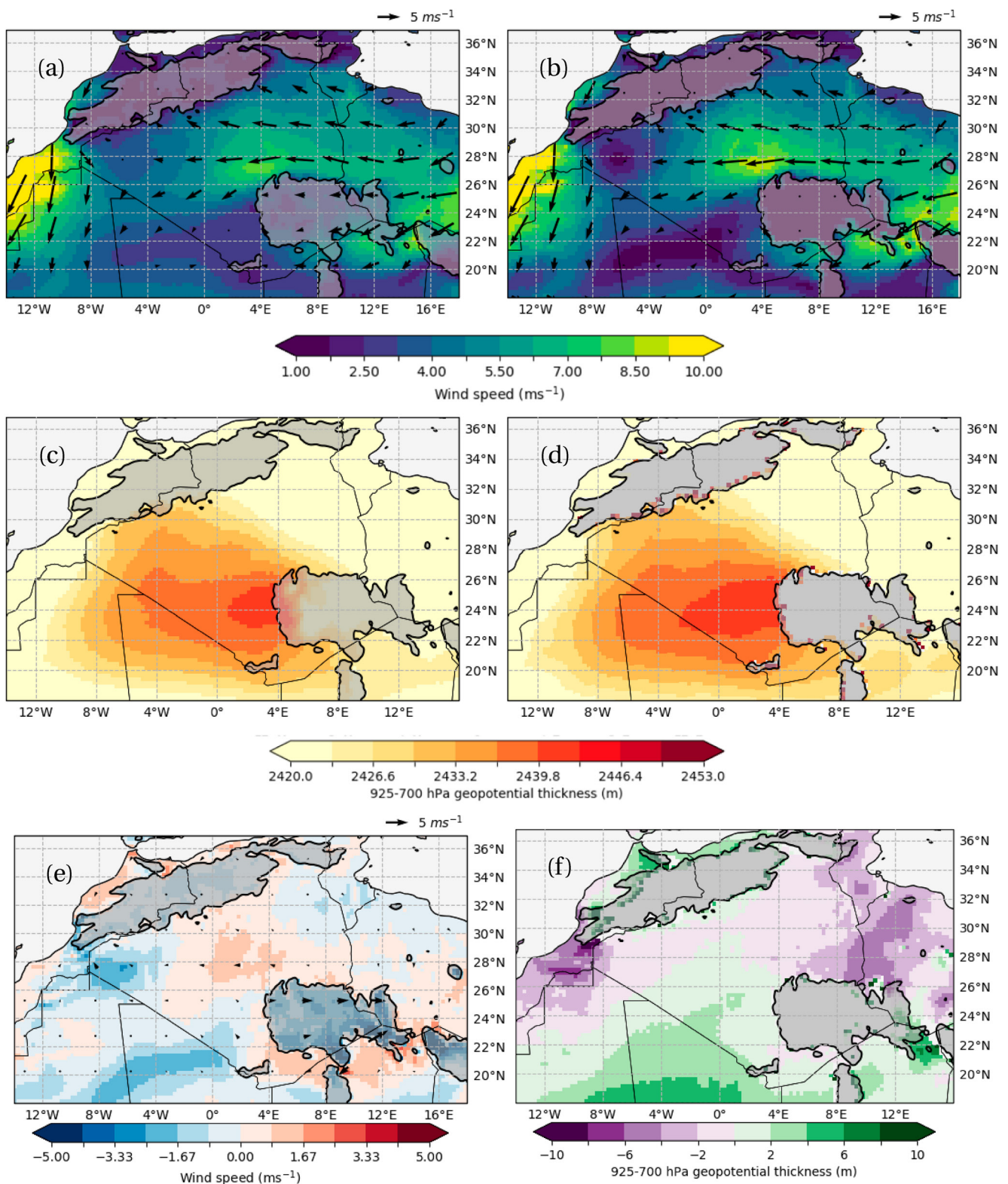


Figure 1. Comparison between ERA5 (left) and 12 km horizontal resolution Unified Model remapped onto the ERA5 horizontal grid (right). Filled contours in (a) and (b) represent 925 hPa wind speeds (m s^{-1}). Filled contours in (c) and (d) are the thickness of the 925–700 hPa geopotential height layer (m). (e) and (f) show the difference between the two fields (UM minus ERA5) for the 925 hPa wind field and 925–700 hPa geopotential thickness, respectively. Both quantities are averaged over June, July and August of 1997–2007. Regions above 700 m elevation are contoured and shaded in gray.

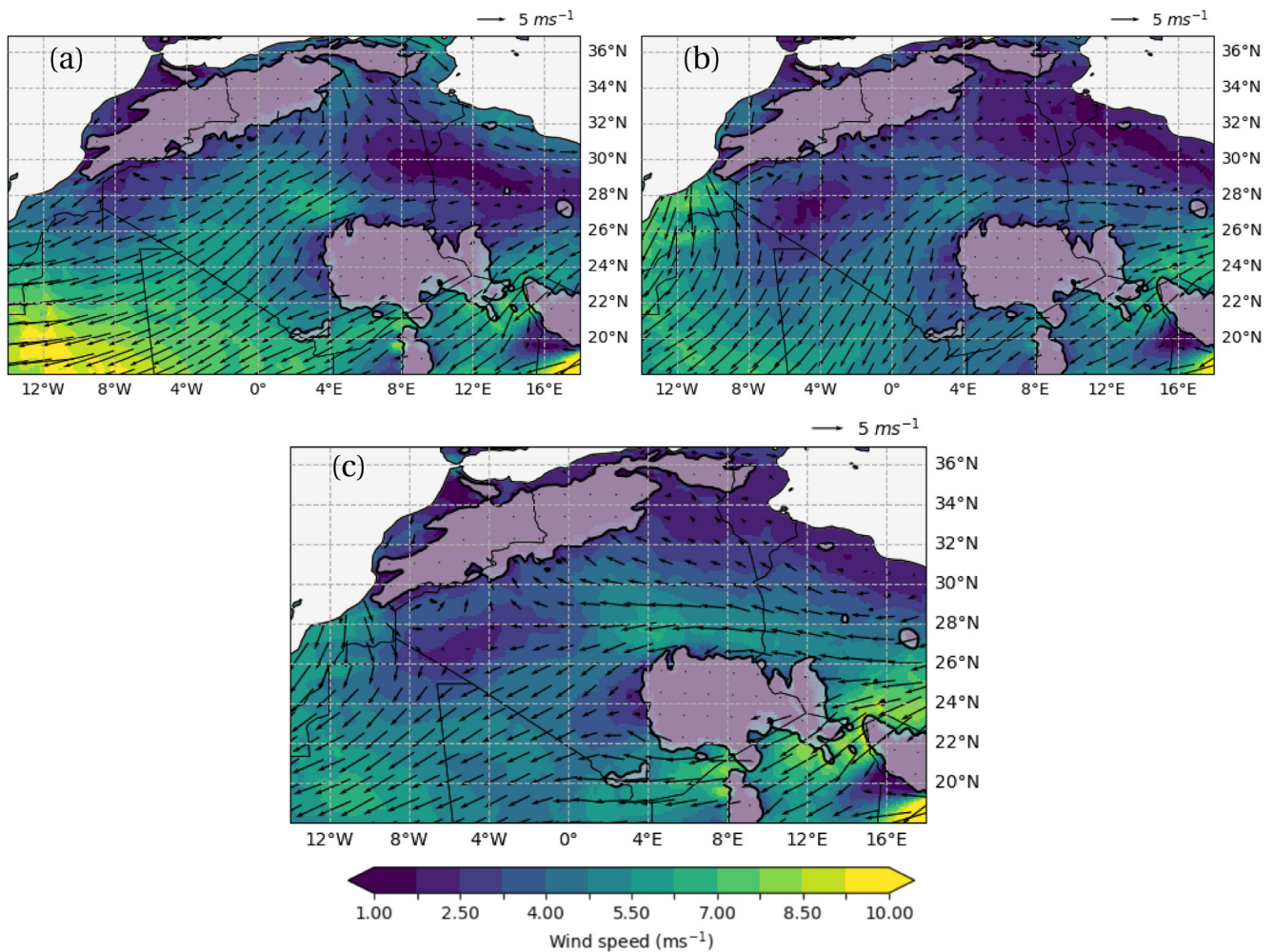


Figure 2. Mean 925 hPa control experiment wind speeds (m s^{-1}) outside of summer, including (a) DJF, (b) MAM and (c) SON for the period 1997–2007. Regions above 700 m elevation are contoured and shaded in gray.

Washington, 2014; Roberts et al., 2017). ERA5 is not used for lateral boundary conditions in this research as the UM infrastructure does not currently support it.

A close match between the large-scale wind field is evident in comparing the UM and ERA5 (Figures 1a and 1b). Northeasterlies enter the region of the SHL via a gap between the Atlas and Hoggar mountain ranges, as well as Atlantic inflow from the northwest. A minimum in wind speeds occurs at 22°N within the climatological ITD. The highest winds are found along the Atlantic coast where a persistent coastal LLJ linked to the Azores High and SHL overlies the Canary Current (Soares et al., 2019). Crucially for the purposes of this project, the UM accurately reproduces a wind speed maximum in central Algeria, evident in both the reanalysis and surface observations (Chellali et al., 2011). Wind speeds in the core of this maximum are 1–1.5 m s^{-1} higher in the UM compared to ERA5 (Figure 1e), which may be due to a deeper SHL (Figures 1c and 1d), driving a sharper pressure gradient through central Algeria (Figure 1f) as well as due to the higher spatial resolution of the UM (12 km compared to 30 km in ERA5).

An interesting feature of the Tidihelt jet is that it appears as a small local wind maximum year-round (Figure 2), including when the SHL is situated much further south than its central Saharan position in JJA (Lavaysse et al., 2009). This shows that a local control is important for the position of these high winds, rather than simply being the result of synoptic pressure patterns. Nonetheless, the jet is at its strongest in JJA (Figure 1b). Whereas in DJF, MAM, and SON the top of the jet feature is situated at 850–800 hPa, during JJA a much deeper boundary layer appears to mix momentum from the jet to greater heights of 750–700 hPa (not shown).

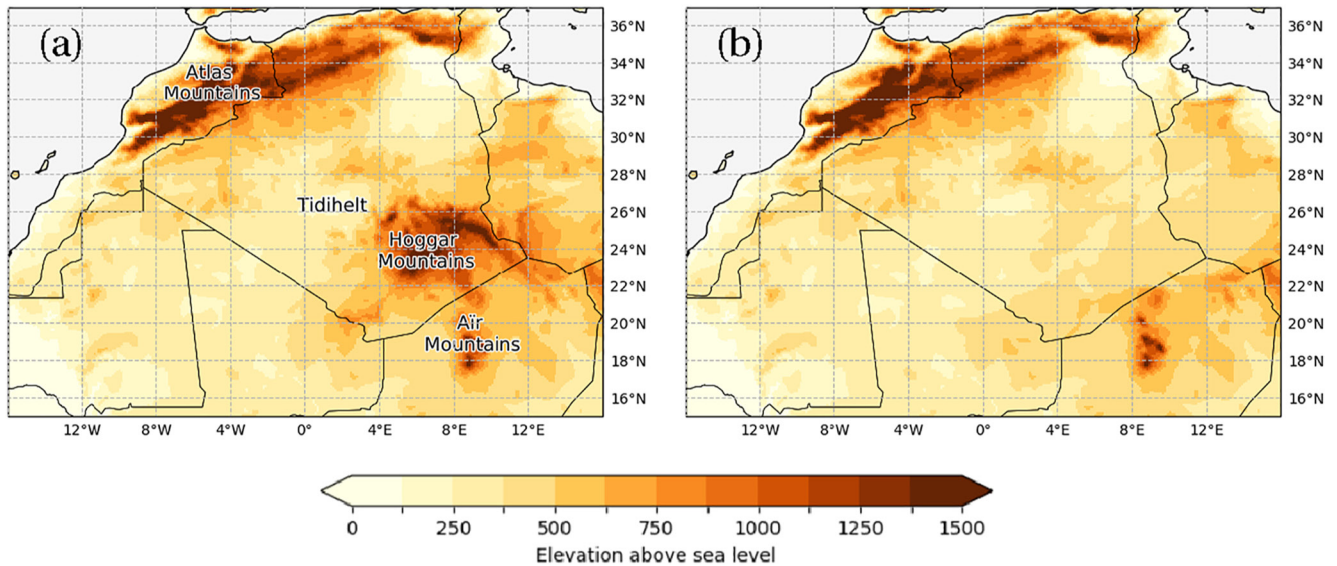


Figure 3. Representation of orography as elevation above sea level in the 12 km UM simulations for the control experiment (left) and the FLATHOGGAR experiment (right). Relevant geographical features are labeled in (a).

2.4. Orography Experiments

Two simulations are run. In the first (CONTROL, Figure 3a), the UM is run with full orography over the limited area domain. In the second run (FLATHOGGAR, Figure 3b), the region encompassing the Hoggar mountains is smoothed to a uniform level. Unlike Birch et al. (2012), we do not remove the Air mountains at 19°N, 9°E as our goal was to isolate the role that mountains adjacent to the Tidielt region have upon winds there; furthermore, the Air Mountains are an important site of late summer convective triggering (see Redl et al. [2015], Figure 6 therein) which could have an impact upon the low-level monsoon circulation. The same lateral boundary conditions are supplied by ERA-Interim in both experiments, meaning that although the removal of the Hoggar mountains may influence the large-scale flow beyond the limited area domain, this effect is not accounted for in this paper.

One approach tested for flattening the Hoggar region was to apply a mask and level all terrain therein to a maximum of 350 m above sea level. This introduced sharp horizontal discontinuities, especially toward the east of the domain around 12–14°E which produced local wind acceleration in the simulations. The solution adopted here is to smooth the mountains by cloning terrain from the lowlands in the central Saharan Erg Chech and El Djouf (4°W–0°E) over the Hoggar plateau, introducing a more gradual incline toward the higher elevation of eastern Algeria and Libya. Terrain from the western Sahara is selected for cloning as it is homogeneous in elevation over spatial scales of hundreds of kilometers and therefore best approximates a flat sand sheet with no orography.

Edits are applied to a 1 km resolution topography dataset prior to generating the UM ancillary files describing the mean and sub-grid properties of the orography. The effects of flow blocking, orographic form drag and orographic gravity wave drag are then calculated consistently following the method described in Walters et al. (2019) (see Sections 2.6 and 3.5 therein). Orographic effects at the smallest scales (at which buoyancy effects are negligible) are represented by an effective roughness length (i.e., indirectly) while sub-grid orographic effects at larger scales up to the model resolution are represented with a drag scheme originally developed by Lott and Miller (1997) with slight modifications described in Section 3.5 of Walters et al. (2017). No changes are made to albedo, which is tested in more detail in Birch et al. (2012) and shown to exert a smaller influence on the boundary layer than the orography itself. Surface roughness is also not edited in these experiments beyond the effective roughness length described above.

2.5. Composite Method

The composite method in this paper selects high northeasterly surface wind days with visible dust emission. Compositing is used in this analysis rather than averaging over the whole simulation for two reasons. Firstly,

although northeasterlies are the most common wind regime in the Tidihelt region, other wind regimes are active through summer due to occasional incursions from monsoon winds and Atlantic inflow. Secondly, high wind days are disproportionately important for dust emission. The bulk of the results presented in this paper are obtained from a comparison of composited days between the two experiments. An analysis of the overall effect on the potential for dust emission across all days is presented in Section 4.4, however.

A sub-domain within the limited area of the model simulations is delineated and corresponds to the Tidihelt Depression in central Algeria, described in more detail in Caton Harrison et al. (2019). The boundaries are 25–28°N, 1.5°W to 3°E (the box region in Figure 5). Henceforth, this is referred to as the TID region.

Mornings with high surface winds and visible local LLJ-linked dust emission in the control experiment TID region are selected for compositing. Dust emission is not computed in the model simulations, hence information about emission must be obtained from the contemporaneous satellite record. The period of June, July and August (JJA) 2004–2007 is used as this contains an overlap between the period for which UM data is available (1997–2007) and the period for which SEVIRI dust tracking has been performed (2004–2017). Each selected day must fulfill the following conditions for the day to count as a dust day:

1. At least 500 total dust pixels visible between 05:00 and 13:00 UTC in SEVIRI in the TID region which the algorithm from Caton Harrison et al. (2019) identifies as LLJ dust
2. Any dust observed is freshly emitted (within the same morning)
3. Mean control Experiment 10 m wind speed within the TID region exceeds 7 m s^{-1}
4. Mean control Experiment 10 m wind direction within the TID region for the day is between 0° and 90°

A wind direction constraint is included in order to limit the analysis to a northeasterly wind regime associated with the prevailing dry Harmattan. As identified in Section 2.3, the existing analysis of UM performance in Allen and Washington (2014) indicates that fidelity is excellent for northeasterly jets. On the other hand, it is relatively poor for southwesterly jets embedded within the monsoon.

The 30 days with the highest mean wind speed and which also fulfill the conditions above are selected for inclusion within the composites. Composites are averaged over 05:00–12:00 UTC to target a period in which both the core strength of the jet peaks and the mixing of momentum to the surface occurs. Note that an extra hour is included on the end of the SEVIRI dust observation window as occasionally dust plumes emitted in the mid-morning do not become visible until around midday.

The 7 m s^{-1} wind speed threshold chosen here is conservative compared to estimated dust emission thresholds at surface stations in central and southern Algeria (Cowie et al., 2014), but provides a good sample of days to choose from given the limited time analysis time period of four summers; 46 days fulfilling each composite condition are found, of which the top 30 are selected. For a clearer picture of the likely dust emission threshold for the TID region, an analysis of the relationship between simulated winds on these composite days and observed dust is given in Section 4.4.

3. Synoptic Conditions

Lag-lead composites of 12:00 UTC soundings from In Salah (Figure 4) reveal that a cold northeasterly boundary layer anomaly accompanies strong winds and dust emission over the Tidihelt region. Cold anomalies of -0.5 to -3 K , significant at the 95% level, are observed up to 700 hPa through from Day -3 to Day $+3$. By Day -1 there is a significant northeasterly anomaly of 4.8 m s^{-1} at 925 hPa, backing to northerly at 700 hPa. The coldest layer is found at 925–850 hPa on Day 0 along with a wind anomaly of 5.6 m s^{-1} at 925 hPa and a 3.6 m s^{-1} anomaly observed at the surface level of 982 hPa. Days $+1$ to $+3$ see a continued cold anomaly with winds backing more northerly.

Patterns in the fields from the UM control experiment map on well to observations from Figure 4 and reveal the synoptic processes driving the wind anomalies (Figures 5a–5d). A cold anomaly extends from the Mediterranean to central Algeria, advected by northeasterlies which reach their westernmost extent on Days 0 and $+1$ (Figures 5c and 5d). This strengthens winds through the Harmattan LLJ alley into the core of the SHL and also drives an intense warm anomaly on the Atlantic coast by blocking cooler maritime inflow.

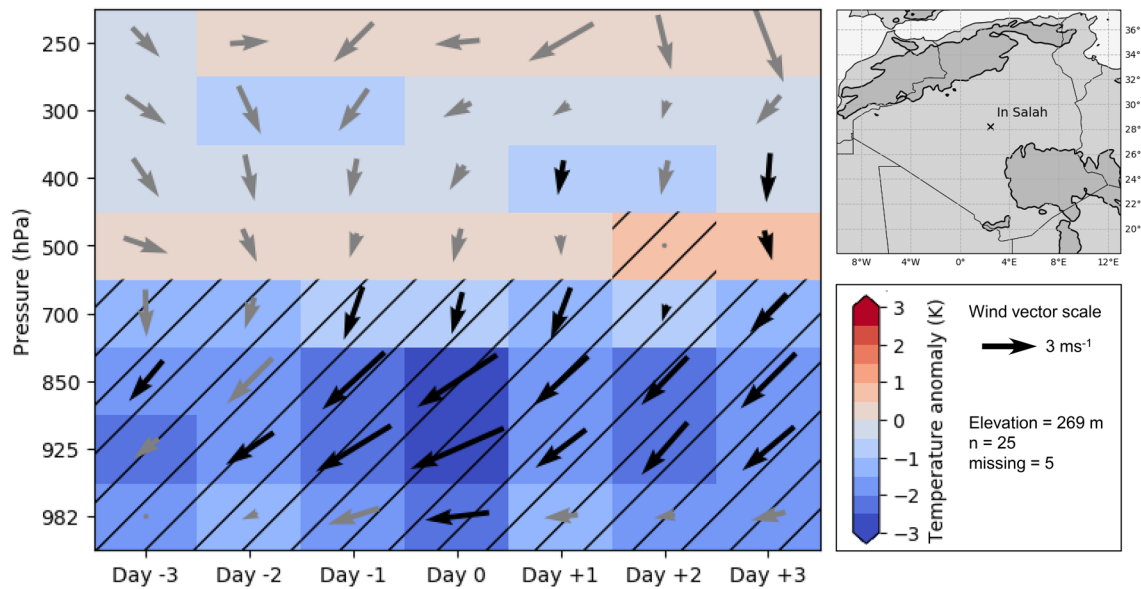


Figure 4. Time versus height composite sonde measurements of temperature anomaly (shaded boxes) and wind speed/direction anomaly seen from a bird's eye view (arrows) taken at 1200 UTC at In Salah relative to the mean for June, July and August 1997–2007. Each column represents a lag relative to the composite event at Day 0. Temperature anomalies significant at the 95% level are hatched. Wind speed anomalies significant at the 95% level are represented in bold. An inset map identifying the location of the sonde launches is shown in the top right.

Intensification of subtropical low-level high pressure over the eastern Sahara associated with intrusion of a mid-latitude trough and cold inflow from the Mediterranean has long been linked with strengthened Harmattan winds (Kalu, 1979, Figures 5.4 and 5.5 therein). Synoptic conditions shown in Figure 5 resemble a typical Mediterranean cold surge event which can persist over North Africa for up to 10 days alongside an enhanced upper tropospheric ridge-trough pattern (Vizy & Cook, 2009). Upper level ridging over the Atlas mountains in the UM simulation is accompanied by a trough over the Mediterranean (Figures 5e–5h) which propagates eastward through the composites. At low levels, a low pressure anomaly is present south of 28°N and east of 0°E which shifts westward from day –2 (e) to day +1 (h). North of 28°N, anomalous high pressure develops and intensifies to a maximum at day 0 (g) over and south of the Atlas mountains, producing conditions associated with a high North African Dipole Index (NAFDI) (Rodríguez et al., 2015).

In the remainder of the paper, we study the low-level circulation patterns for the lag 0 composite days in both the control and FLATHOGGAR simulations.

4. Model Experiment Results

4.1. Wind Speed and Vertical Structure

925 hPa composite winds in the control experiment (Figure 6a) exhibit a maximum northwest of the Hoggar mountains, extending from 6°E to the Algerian border with Mali and Mauritania. Northeasterlies between 56° and 79° account for over 40% of composite winds averaged across the TID domain (Figure 6b). TID is also situated at a confluence with southeasterlies along the western flank of the Hoggar mountains. The northern limb of the SHL circulation is found around northern Mali at 24°N, with northerlies across Mauritania.

A substantial reduction in wind speeds occurs over the Tidihelt region in the absence of the Hoggar mountains (Figure 6c), with mean composite winds within TID dropping from 9.0 to 7.3 m s⁻¹. A slight local maximum nonetheless persists over central Algeria. A shift in the wind regime can be seen over the TID region, with winds in the 56–79° range reduced (Figures 6b and 6d) in favor of easterlies (79–101° on the wind rose), which also prevail over the region previously occupied by the Hoggar mountains. Southeasterlies are no longer evident in southern Algeria and the SHL circulation appears to be shifted southward, with a northern limb extending down to 22°N and reduced northerlies in eastern Mauritania (Figure 6c).

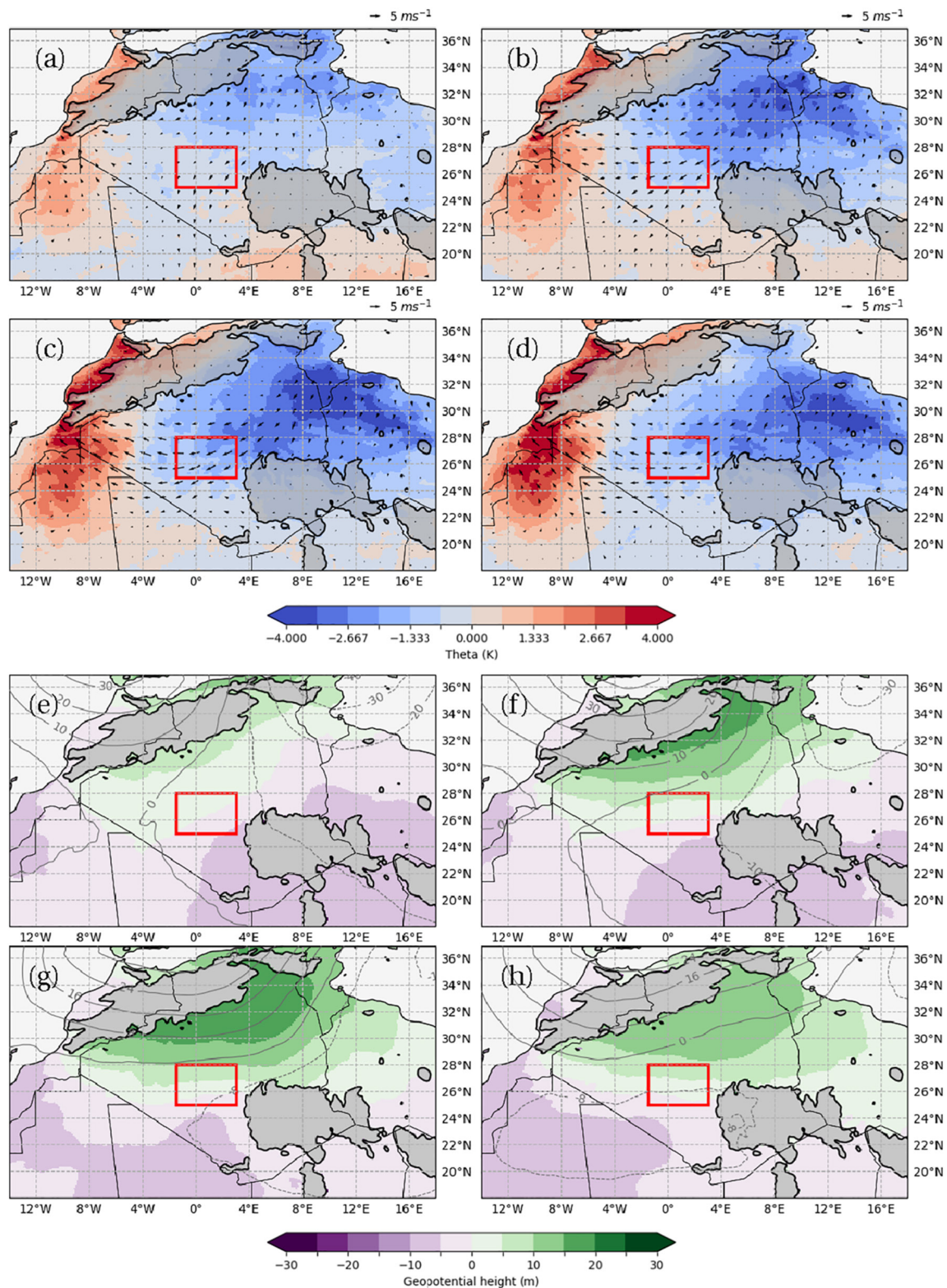


Figure 5. Upper plots (a–d) show control experiment composite anomaly potential temperature at 130 m height (filled contours) with wind vectors relative to the mean for June, July and August 1997–2007, going from day –2 (a) to day +1 (d). Lower plots (e–h) show control Experiment 925 hPa composite anomaly geopotential height (filled contours) and 200 hPa geopotential height (contours, negative where dashed) relative to June, July and August 1997–2007, going from day –2 (e) to day +1 (h). The red box identifies the region from which high wind/dust days are selected for the composite. Regions above 700 m elevation are contoured and shaded in gray.

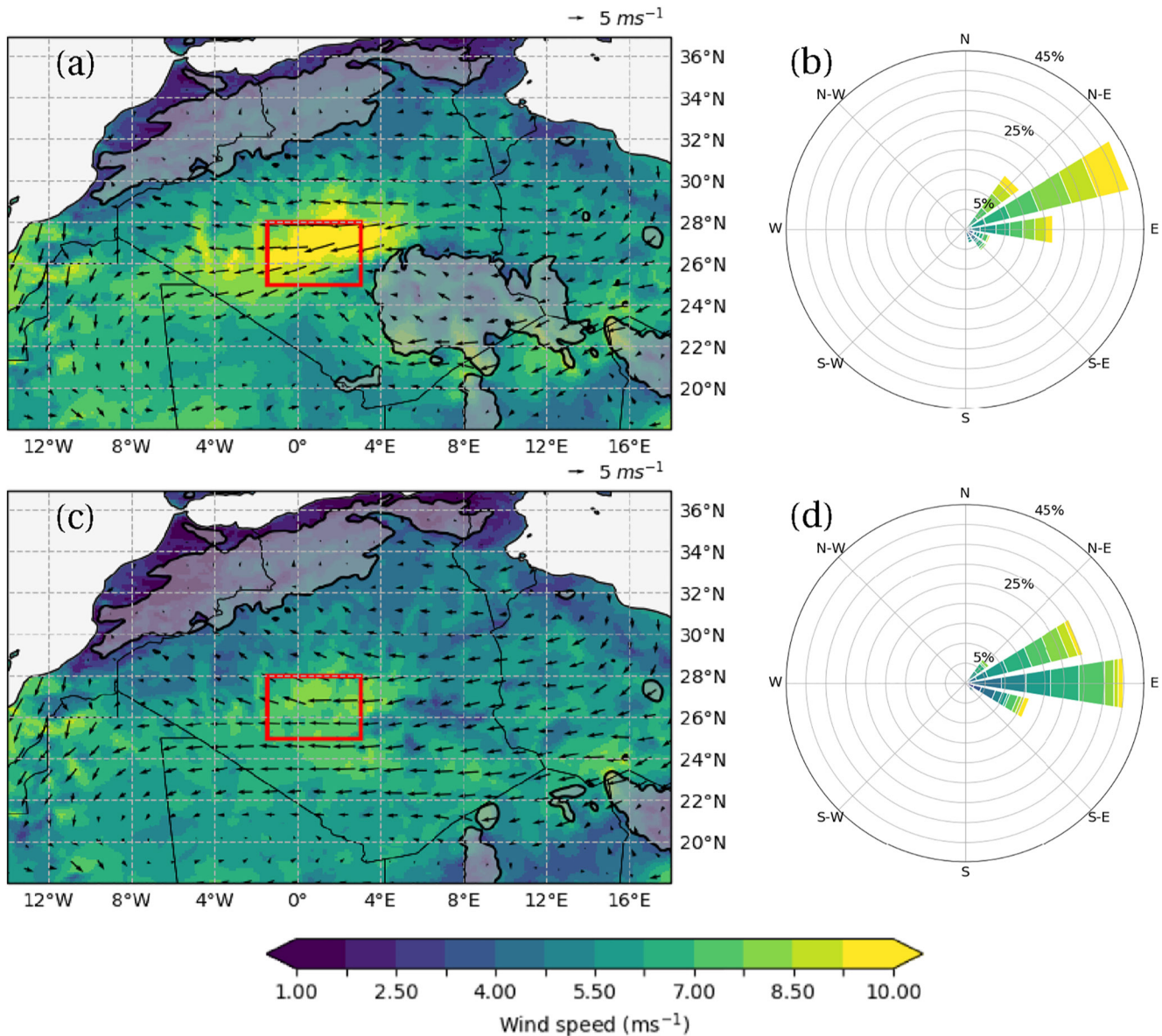


Figure 6. Composite 925 hPa absolute wind speeds (left, filled contours and wind vectors) for the control (upper) and FLATHOGGAR (lower) experiments. Wind roses are shown on the right, calculated from the average of the 925 hPa winds within the composite region (red boxes). Regions above 700 m elevation are contoured and shaded in gray.

It should be noted that a potential drawback of a compositing approach here is that data in the control experiment is selected for high wind speeds, whereas data in the counterfactual FLATHOGGAR experiment is not; removal of orography could affect the timing of high wind events and the wind regime in which they occur and hence cause winds to peak on different days. When the same analysis as in Figure 6 is carried out for the entire dataset instead of composite days, a similar result emerges in a subtler form; the dominant shift is still a reduction of wind speeds proximate to the Tidihelt (by 10.1% instead of the 18.9% obtained with compositing) and a slight preference for easterlies over northeasterlies (not shown). The effect of orography upon modeled winds is therefore greater than usual on days with synoptic forcing driving an intense northeasterly jet. There is no indication, however, that the strongest winds seen on composited control days occur at other times in the FLATHOGGAR results. Further evidence of this may be found in Section 4.4 (Figure 13a) in which non-composited wind speed distributions are compared for the two experiments.

A composite cross section across the TID region in the control experiment reveals that the Tidihelt jet is a low-level nocturnal feature, extending to approximately 1,800 m above sea level at 00 UTC (Figure 7a). The jet core is close to the surface at 1,000 m above sea level or approximately 100 m above the surface. During the day, winds within the boundary layer are well-mixed with a much slower core below 10 m s^{-1} extending up to above 2,000 m above sea level (Figure 7b). Although the nocturnal jet extends from 1 to 6°E , the highest winds are found south of the Tademaït Plateau in the low-lying Tidihelt Depression, corresponding to the TID region ($25\text{--}28^\circ\text{N}$, 1.5°W to 3°E). In the FLATHOGGAR experiment (Figures 7c and 7d), the jet core is significantly eroded and less clearly defined, although the winds are still accelerated nocturnally (Figure 7c).

4.2. Leeward Circulation

The difference between the two experiments at 850 hPa reveals a circulation pattern centered over the TID (Figure 8). The circulation has a northern limb of northeasterly anomalies through central Algeria and a southern limb of southeasterlies and easterlies in the lee and over the Hoggar mountains (Figure 8b). This is associated with a geopotential height perturbation of -15 to -20 m over the TID region at 850 hPa (Figure 8a), with significant differences of 5–10 m as far west as the Atlantic coast.

East-west cross sections through the Hoggar mountains indicate a diurnal variation in the circulation pattern. In both the control (Figures 9a–9d) and FLATHOGGAR (Figures 9e–9h) experiments, easterlies persist nocturnally, albeit weakened on the western slopes in the control. During the day, however (Figures 9c and 9d), easterlies drop to zero between 2° and 5°E in the control, whereas in FLATHOGGAR they are maintained at $3\text{--}5 \text{ m s}^{-1}$ (Figures 9g and 9h). This suggests an upslope wind in the control experiment driven by enhanced sensible heat fluxes over the elevated terrain driving a thermally direct circulation (Wolyn & Mckee, 1994; Zängl & Chico, 2006). In this instance, however, no actual upslope winds develop as the background flow is too strong. Differences between the meridional circulation are more stark; whereas in FLATHOGGAR a mild southerly component is present at 06:00 UTC (Figure 10f) and eroded entirely during the day (Figure 10g), in the control experiment a southerly flow develops overnight over the peak of the Hoggar and reaches a maximum of up to 5 m s^{-1} at 06:00 UTC (Figure 10b) at which point it is located over the western mountain lee slopes. The result is a net southeasterly into the Tidihelt Depression. During the day, this flow weakens and shifts further westward (Figure 10c).

The Hoggar mountains are subject to intense heating during the day. The difference between potential temperature fields of the two experiments becomes greatest at 12:00 UTC (Figure 11c), with a peak over the summit extending up to 3,000 m in a dome shape. During the night, this heating perturbation shifts westward (Figure 11a, 11b, and 11d) and is situated within a residual layer above the surface over $0\text{--}5^\circ\text{E}$. This elevated heating due to the presence of the Hoggar mountains induces a horizontal temperature gradient over the plateau (about 1,500 m elevation) relative to the low lying Sahara to the west (about 300 m elevation). A gradient between the cooler maritime west and the SHL exists in the absence of the mountains (not shown) but is greatly intensified when elevated terrain is present. The existence of elevated heating and baroclinicity suggests that the Hoggar mountains may be capable of setting up a thermal low or trough within the much broader SHL, deepening and extending it.

The Tidihelt jet is a nocturnal phenomenon; 925 hPa composite winds in the Tidihelt region reach their maximum at midnight UTC and minimum at 13:00 UTC, whereas the minimum mean 925 hPa geopotential height in the lee of the Hoggar mountains occurs at 17:00 UTC (not shown). This temporally shifted relationship aligns with the theoretical behavior of heat lows which develop to their lowest central pressure in the afternoon and evening. Being out of quasi-geostrophic balance, however, the peak winds and relative vorticity occur several hours after the pressure minimum (RÁCZ & Smith, 1999; Spengler & Smith, 2008). The exact timing of the peak in low-level winds can also depend on the Coriolis parameter and its effect on inertial oscillation (RÁCZ & Smith, 1999); this is tested by Heinold et al. (2015) who show that a later timing of maximum supergeostrophy (i.e., closer to sunrise) is favored at 20°N compared to 30°N , with the Tidihelt at a latitude of about 26°N . A daytime minimum in low-level winds is driven by intense mixing of the convective boundary layer, which inhibits horizontal flows (Parker et al., 2005). Furthermore, it is plausible that the background easterlies act to shift the center of the heat low westward to its mean position seen in Figure 8a, similar to the effect of background easterlies on the Australian heat trough (Spengler et al., 2005).

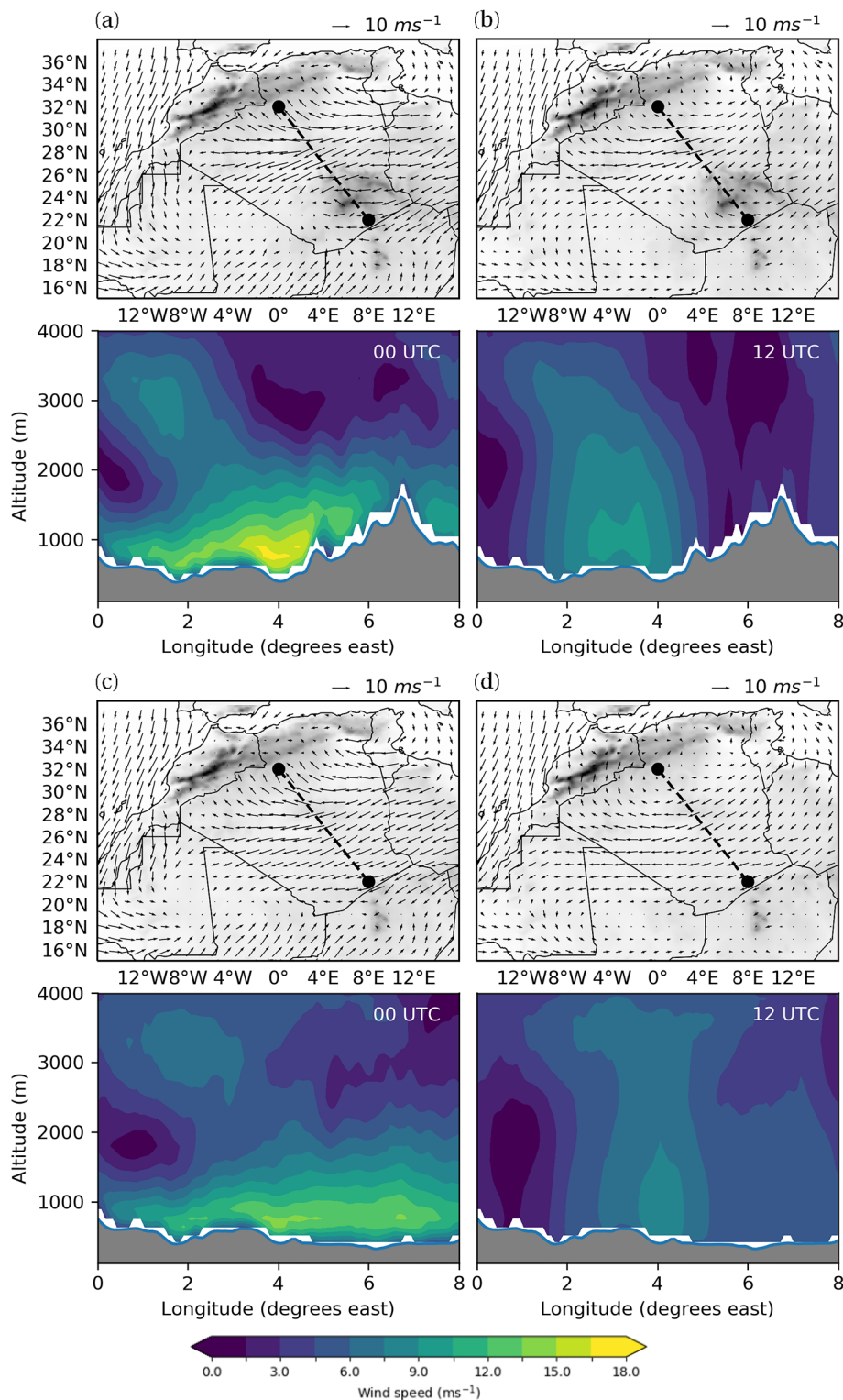


Figure 7. Composite cross sections of wind speed (filled contours) calculated across the axes plotted as dashed lines on the horizontal wind field maps above each cross section, in which composite wind bars at 925 hPa are also plotted and orography shaded in the background. Composite times of 00 and 12 UTC are shown for the control experiment (a) and (b) and the FLATHOGGAR experiment (c) and (d). Model orography for both experiments is shaded in dark gray over the composite cross sections.

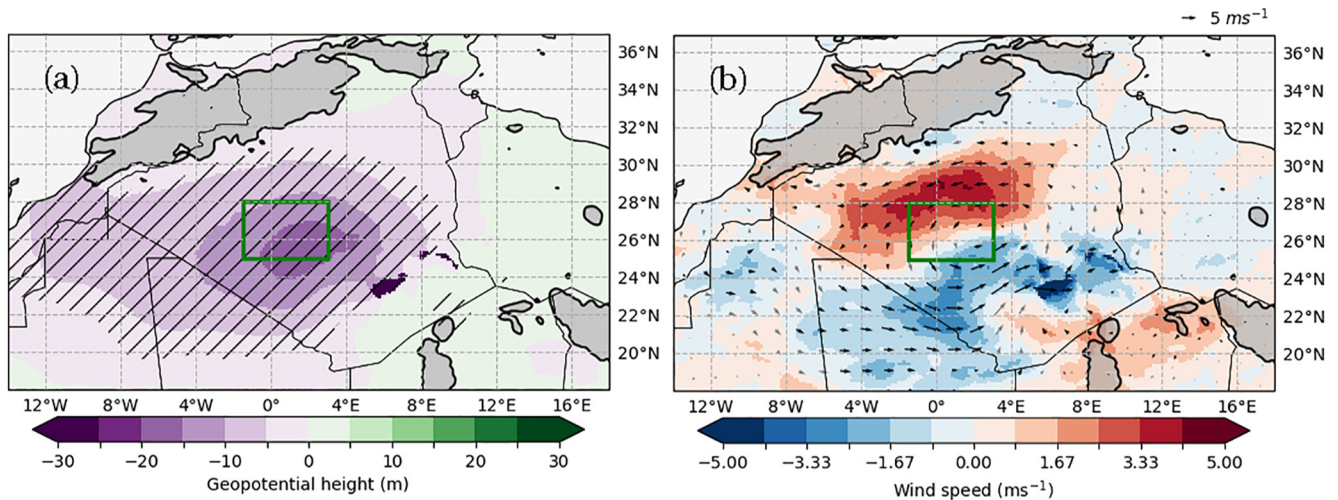


Figure 8. Control minus FLATHOGGAR experiment composite (a) 850 hPa geopotential height and (b) 850 hPa wind field (wind speed as filled contours). Significant geopotential height differences at the 95% level are hatched. Significant wind speed differences at the 95% level are shown as bold black wind vectors. The green box identifies the region from which high wind/dust days are selected for the composite.

4.3. Geostrophic Wind Analysis

To test the role that elevated heating could have upon winds in the Tidihelt notwithstanding any additional dynamic effects, we estimate the geostrophic winds induced by a heating anomaly equivalent to the difference between the control and FLATHOGGAR experiment. It should be noted that as the diabatic heating and cyclonic circulation are out of phase the real Tidihelt jet is not in geostrophic balance; furthermore its peak core wind speeds are subject to supergeostrophy due to inertial oscillation. These estimates instead serve to identify the expected spatial pattern of winds induced by thermal forcing for comparison with Figure 8.

Atmospheric thickness is estimated for the 925–700 hPa layer from the temperature profile of the control and FLATHOGGAR experiments to account for the heating effect of the Hoggar mountains. Assuming hydrostatic balance, the atmospheric thickness in a given layer corresponding to a temperature profile is given by the hypsometric equation:

$$z_2 - z_1 = \frac{R_d}{g} \int_{p_1}^{p_2} T_v d \ln p \quad (1)$$

in which z_1 and z_2 are the lower and upper heights of the layer between pressure levels p_1 and p_2 (925 and 700 hPa in this instance), R_d is the gas constant for dry air, g is gravity, and T_v is the virtual temperature.

The difference between the estimated atmospheric thickness of the two experiments (Figure 12a) shows a thickness perturbation of over 10 m centered over the lee of the Hoggar mountains, in close resemblance to the 850 hPa pattern (Figure 8a). Negative differences (warmer temperatures in the control) extend through central Algeria and into Mali, with evidence of positive differences (cooler temperatures in the control) along the west coast. This pattern is comparable to the SHL itself (Figure 1d) but its core is situated slightly further east over the Hoggar mountains themselves. Nonetheless, these results suggest the presence of the mountains is capable of introducing elevated heating which could deepen or extend the SHL.

To understand the effect such heating could have upon the winds, we compute the geostrophic wind change induced if geopotential heights at an arbitrary level (within 925 to 700 hPa) were lowered by the thickness differences shown in Figure 12a. The results show a circulation pattern centered around the thermal low (Figure 12b), with peak geostrophic winds in excess of 5 m s^{-1} within and upstream of the TID domain where the pressure gradient peaks. This circulation closely resembles the spatial structure of the wind difference between the control and FLATHOGGAR experiments at 850 hPa (Figure 8b). Such a similarity suggests that heating alone is capable of explaining the pressure pattern and that a local maximum in winds over the Tidihelt is the result of a thermodynamically forced nocturnal LLJ.

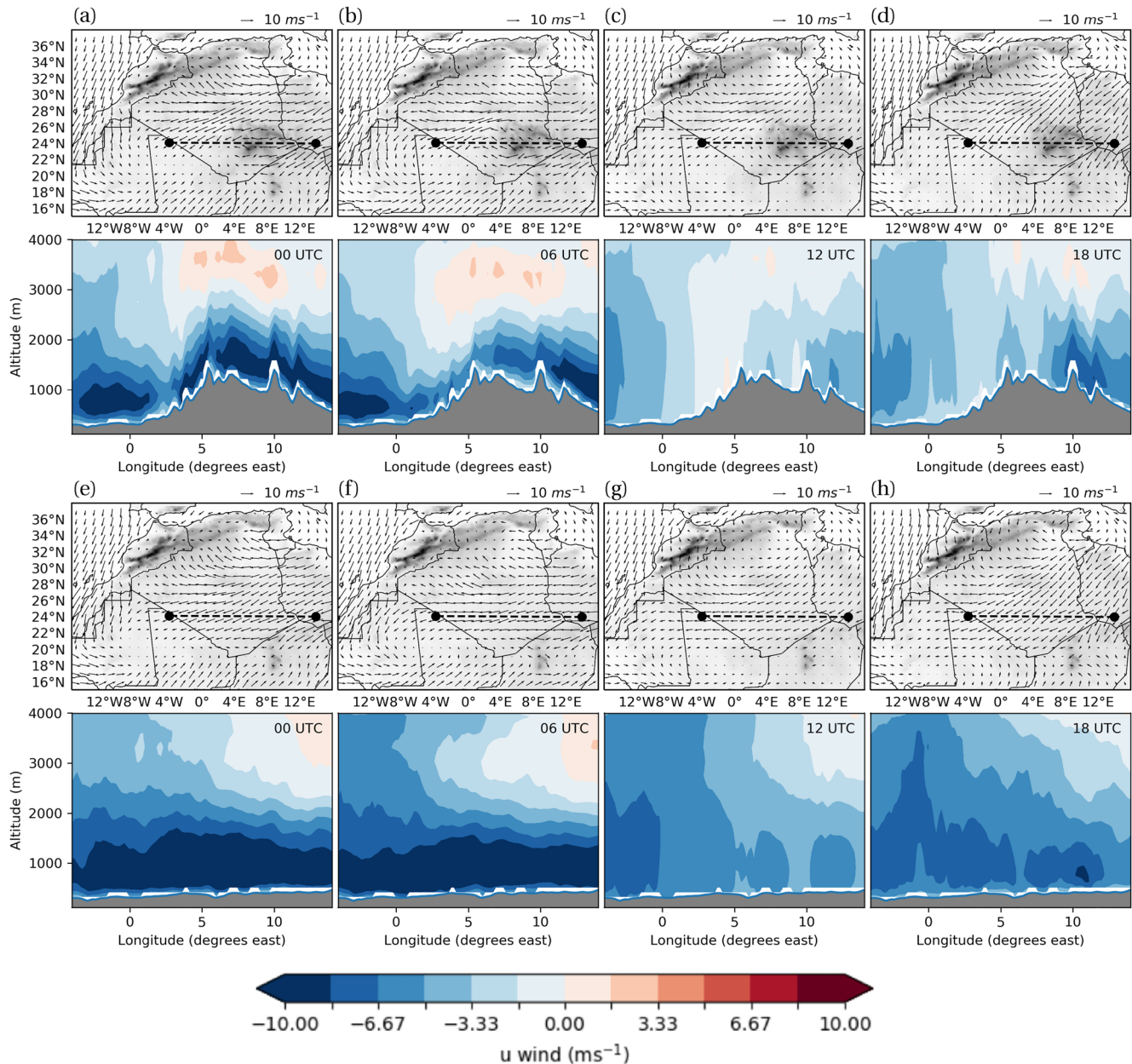


Figure 9. Composite cross sections of u winds for the control (a)–(d) and FLATHOGGAR (e)–(h) experiments. Cross sections are calculated across the axes plotted as dashed lines on the horizontal wind field maps above each cross section, in which composite wind barbs at 925 hPa are also plotted and orography shaded in the background. Composite times of 00 (a), (e); 06 (b), (f); 12 (c), (g); and 18 UTC (d), (h) are shown. Model orography for both experiments is shaded in dark gray over the composite cross sections.

Our explanation for lee cyclogenesis over and west of the Hoggar mountains does not rely on the generation of an upstream anticyclone at low levels to enhance northeasterly winds as shown in the comparable idealized model experiment of Semazzi and Sun (1997). In contrast with their analysis, our composite appears to show only minor differences in anticyclonic circulation on the windward side of the Hoggar mountains (Figure 8a) although an enhanced anticyclonic return flow is observed atop the leeward circulation, especially above 500 hPa. Instead, the results suggest that the enhanced elevated heating of the boundary layer is the primary control upon the deepening of the eastern SHL and enhancement of the winds through the Tidihelt.

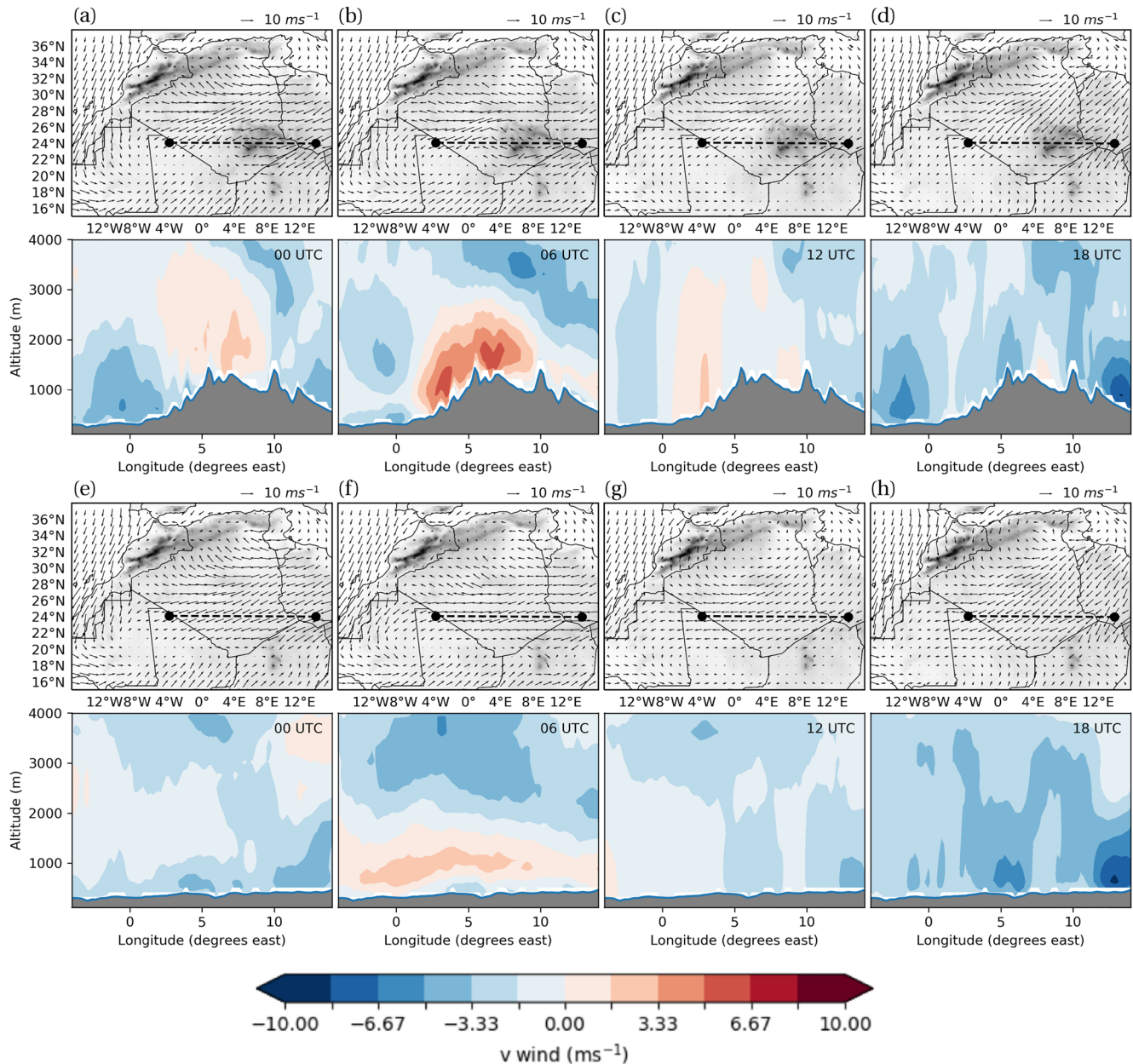


Figure 10. Composite cross sections of v winds for the control (a)–(d) and FLATHOGGAR (e)–(h) experiments. Cross sections are calculated across the axes plotted as dashed lines on the horizontal wind field maps above each cross section, in which composite wind barbs at 925 hPa are also plotted and orography shaded in the background. Composite times of 00 (a), (e); 06 (b), (f); 12 (c), (g); and 18 UTC (d), (h) are shown. Model orography for both experiments is shaded in dark gray over the composite cross sections.

A low level lee circulation over central and southern Algeria appears in each climatological season (not shown), suggesting it is a stationary feature which helps maintain the elevated winds in the Tidielt through the year (Figure 2), with peak strength when the lee circulation is collocated with the SHL in summer.

4.4. Role in Dust Emission Frequency

The Tidielt depression is an important and frequently activated dust source (Ashpole & Washington, 2013; Catton Harrison et al., 2019; Schepanski et al., 2007). Our results show that the Hoggar mountains play an important role in accelerating low level winds over the region. We hypothesize that the mountains could therefore be partly responsible for the prominence of this dust source, meaning they are important for both erosivity on their leeward

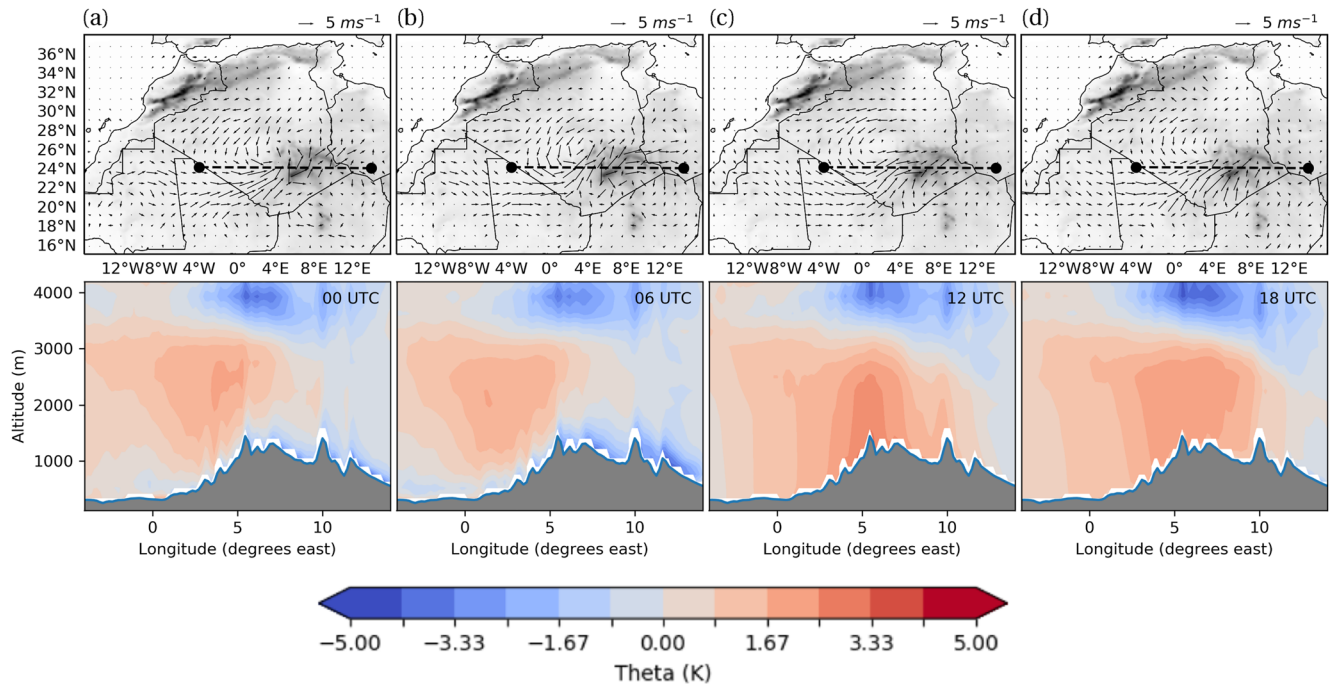


Figure 11. Composite cross sections of air potential temperature for the control minus FLATHOGGAR experiments. Cross sections are calculated across the axes plotted as dashed lines on the horizontal wind field maps above each cross section, in which control minus FLATHOGGAR composite wind barbs at 925 hPa are also plotted and orography shaded in the background. Composite times of (a) 00, (b) 06, (c) 12, and (d) 18 UTC are shown. Model orography from the control experiment is shaded in dark gray over the composite cross sections.

flank. To test this hypothesis, an estimate of the relationship between wind speeds and dust emission is needed. To achieve this, we compare simulated wind speeds with satellite observations of LLJ dust plumes. Unlike previous results, no compositing is applied in this analysis as the aim is to estimate the net effect of orography upon dust emission conditions. Results are instead calculated from all model output from JJA 2004–2007 between the hours of 05:00 and 13:00 UTC (i.e., when freshly emitted LLJ dust is visible to satellite).

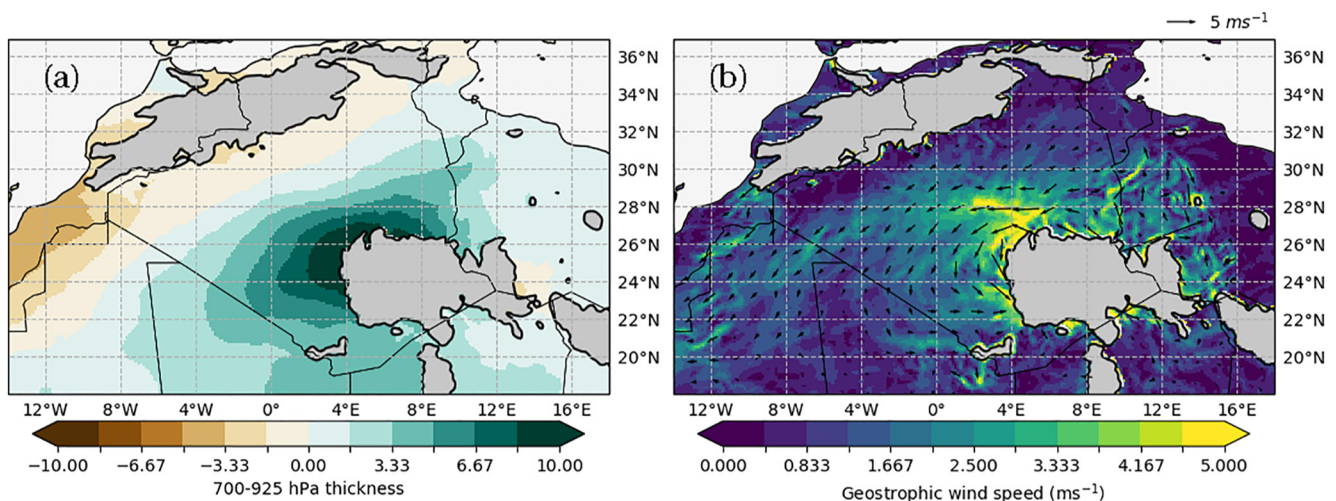


Figure 12. (a) Estimated 925–700 hPa geopotential thickness difference given the difference in the temperature profile between the control and FLATHOGGAR experiment, averaged across the June, July, and August 2004–2007 period, calculated with Equation 1. (b) Geostrophic wind speed increase from the FLATHOGGAR to the control experiment which would be induced by a lowering of geopotential height contours by the amount shown in (a).

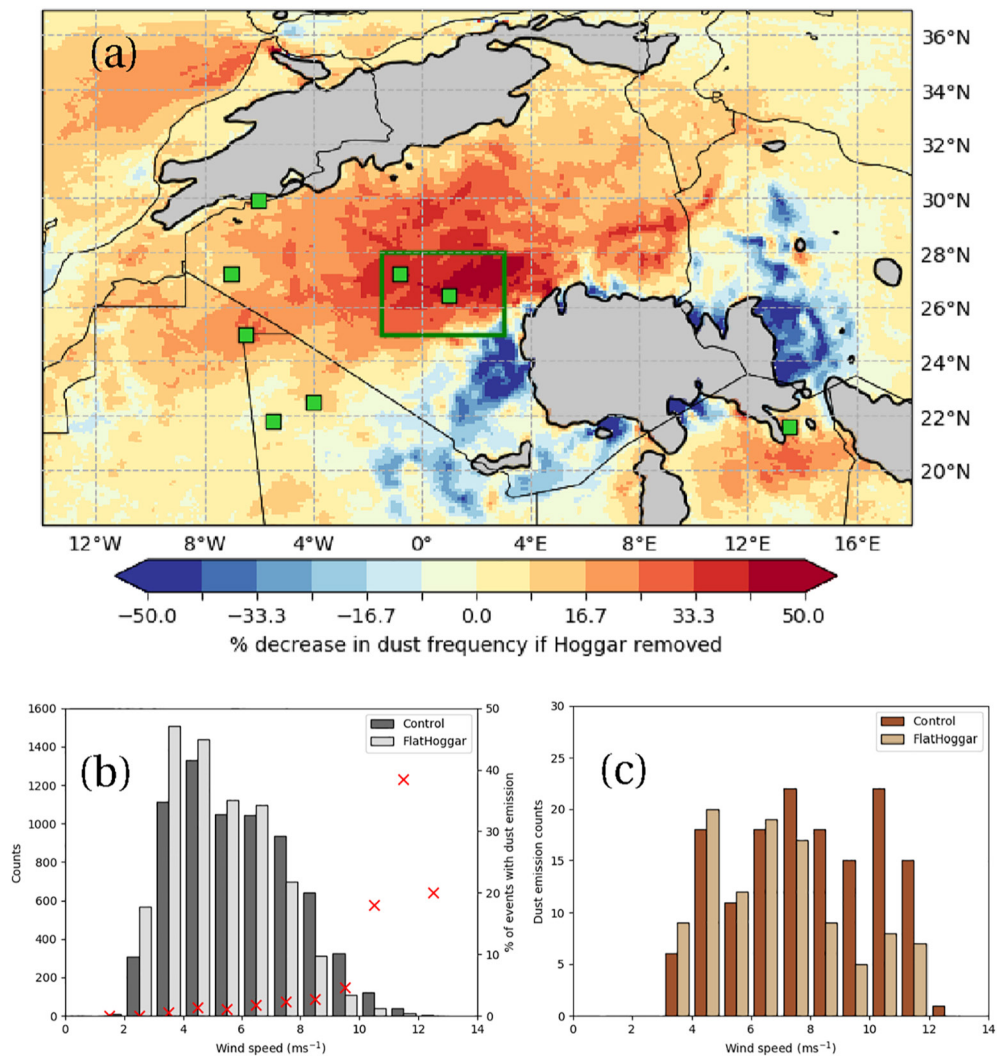


Figure 13. (a) Map of estimated percentage decrease in the frequency of dust emission events if the influence of the Hoggar mountains on the low-level wind field were removed, with a green box identifying the TID domain. Filled green squares show the approximate locations of important LLJ dust sources. In (b), the distribution of hourly composite mean wind speeds in the TID region in the control (dark gray) and FLATHOGGAR (light gray) experiments is shown. The percentage of events which are accompanied by an LLJ Tidihelt dust emission event in SEVIRI is plotted as a red cross for each wind speed bin. (c) shows counts of such emission events in SEVIRI in the TID domain for the control experiment (dark brown) and an estimate of what those counts would be in the FLATHOGGAR experiment given the change in frequency for that wind speed bin (light brown). Model and satellite data is obtained from 0500 to 1300 UTC on all 2004–2007 JJA days.

The method for distinguishing LLJ dust from CPO dust in SEVIRI imagery is described in Caton Harrison et al. (2019). In brief, the timing of emission, plume geometry and distance from deep convection is combined in a multiple regression model to assign a value from 0 to 1 to each discrete dust plume masked in SEVIRI data, with higher values indicating a higher probability of being LLJ-associated (other plumes are assumed to originate from convective CPO activity).

Here, we count dust emission events over the Tidihelt region and assign them to a wind speed bin corresponding to the mean 10 m wind speed simulated over the TID domain for the timestep at which the dust is observed. Dust counts are obtained as hourly totals and compared to hourly UM values. Only LLJ dust emitted the same day and within the TID domain is included. In addition, if the sum of cloud pixels (identified where BT 10.8 μm < 270 K, following Caton Harrison et al. [2019]) in the domain for the hours of 02:00 and 18:00 UTC exceeds 500, the day is considered cloud masked and skipped. The results of this analysis (Figure 13b, dark gray bars, with dust frequency as red crosses) give an approximation of the relationship between simulated wind speed in the control

and observed LLJ dust emission across JJA 2004–2007. The most commonly occurring wind speeds are in the 3–5 m s⁻¹ range, but the winds associated with the highest frequency of dust emission events are found in the 10–12 m s⁻¹ range. This exponential increase in dust emission frequency at higher wind speeds is consistent with the theoretical cubic dependence of dust emission on surface wind speed (Marticorena & Bergametti, 1995). As lower wind speeds are much more common, the counts of dust events in each bin are more even (Figure 13c, dark brown) relative to the distribution of frequencies for each wind speed bin in Figure 13b. For example, although the frequency of dust emission events is quite low in the 4–5 m s⁻¹ range (Figure 13b), the total number of emission events for this bin in the control experiment (Figure 13c) is comparable to that for the 10–11 m s⁻¹ range as there are so many more occurrences of the former wind speed. Note that the very highest wind speed bin with any data (12–13 m s⁻¹) has only 16 occurrences in the control experiment, which may explain why the dust emission frequency drops off again here.

The FLATHOGGAR experiment is observed to shift the 10 m wind speed distribution within the TID domain in favor of lower wind speeds (Figure 13b, light gray bars), with the largest differences found in the high tail; for example, wind speeds in the 8–9 m s⁻¹ range decrease by over 50%. To estimate the effect of this upon dust emission in the Tidihelt, we assume the relationship between wind speed and dust emission holds as a constant between experiments and adjust the frequency of dust emission in each wind speed bin accordingly. For example, 2.8% of wind speed events falling into the 8–9 m s⁻¹ wind speed bin have an LLJ emission event observable in SEVIRI at the same time (18 of 643 counts), so for the FLATHOGGAR the estimated dust counts would be 2.8% of 311 counts, or 8.7 counts. This results in a “simulated” distribution of dust emission counts for the FLATHOGGAR experiment TID region (Figure 13c, light brown bars). As high wind speeds are so important for dust emission, the effect of changes in the tails of the wind speed distribution is substantial; overall the TID region sees an average reduction in dust emission frequency of 31%.

As Figure 8b shows, the effect of the Hoggar mountains on the wind field is not unique to the Tidihelt region. Instead, wind speed changes are observed through the entire LLJ alley. To estimate the wider effect of this shift on the entire model domain, the relationship between wind speed and dust emission identified for the TID region in Figure 13b is assumed to hold across the entire domain, and an estimated FLATHOGGAR dust emission frequency distribution is calculated at each grid box based on the wind speed distribution at that grid box in FLATHOGGAR. The difference between the two experiments' estimated dust emission frequency (Figure 13a) indicates how dust emission frequency in the central and western Sahara might be different in the absence of the Hoggar mountains.

Removing the Hoggar mountains is estimated to have the greatest impact upon dust emission frequency in the Tidihelt region, with percentage decreases over 50% in the 0 to 4°E region most strongly impacted by a combination of background northeasterlies and the leeward circulation observed in Figure 8b. Effects are also observed further north close to the southern foothills of the Atlas mountains as well as over northern Mauritania. To give an indication of the position of this wind speed reduction relative to prominent dust sources, locations with known LLJ-related dust sources from the SEVIRI record are marked in Figure 13a. These are locations where a cluster of at least four SEVIRI pixels are each flagged with 10 or more LLJ dust emission events from June, July and August of 2004–2017 following the method described in Caton Harrison et al. (2019). As well as sources within central Algeria, reduced wind speeds are observed to affect dust emission frequency at sources in northern Mali, Mauritania and western Algeria. By contrast, the mountains are responsible for increased estimated emission frequencies in the immediate lee as well as upstream in western Libya (12–16°E) as a result of flow blocking and an upslope wind flow induced by the elevated heating discussed in Section 4.2, though these regions do not contain clear satellite-observed LLJ dust sources.

This counterfactual set of results comes with caveats. First and foremost, discussing the impact of the mountains in terms of an alternative situation in which those mountains did not exist implies that other conditions would be held constant in such a scenario. Orography is not only responsible for increased erosivity due to accelerated surface winds, however; a large proportion of active dust sources appear to be located close to Saharan mountains around alluvial fans, chotts and sebkhas in the foothills (Middleton & Goudie, 2001; Prospero et al., 2002; Schepanski et al., 2007), suggesting mountains drainage is also a factor in local erodibility. A second caveat is that dust emission thresholds are not constant across North Africa, and a shift in emission frequencies applicable to the Tidihelt does not necessarily hold elsewhere; for example, emission thresholds are thought to be higher in northern Algeria (Cowie et al., 2014). In addition, the lateral boundary conditions are held constant in this

experiment but removal of the mountains may be expected to feed back upon the wider circulation. Lastly, as aerosols are prescribed, the modification to the atmosphere in the FLATHOGGAR experiment does not include dust radiative feedbacks, which may directly alter the local circulation via redistribution of heating within the atmospheric column (Miller & Tegen, 1998) including boundary layer stability and LLJ formation (Miller et al., 2004; Pérez et al., 2006), or indirectly, for example by introduction of ice condensation nuclei (DeMott et al., 2003; Klein et al., 2010; Price et al., 2018). The advantage of the present setup is its relative simplicity, isolating the local impact of the orography directly upon the winds as an empirically associated proxy for dust emission frequency, and the results show that even a moderate shift in the wind speed distribution can have large impacts on dust emission, but a more sophisticated setup is needed to consider the mediating effects of varied land surface conditions, feedbacks on the wider circulation and feedbacks from dust.

5. Summary and Conclusions

The role of the Hoggar mountains in dust-emitting wind conditions within the northeasterly LLJ alley through the central Algerian Sahara has been tested with parallel Met Office Unified Model (HadREM3-GA7.05) experiments. Lateral boundary conditions are supplied by the ERA-Interim reanalysis and a composite method is derived using dust plume observations from SEVIRI to identify days with evidence of both high northeasterly winds and visible LLJ-related dust emission within the Tidihelt region of central Algeria, chosen as a representative dust source. Reanalysis, in-situ observations and model simulations suggest a local maximum in wind speeds exists here, identified in this research as the Tidihelt jet.

High wind and dust conditions within the Tidihelt during boreal summer are associated with a long-lived northeasterly cold anomaly within the boundary layer. This is in turn linked to Mediterranean inflow from an intensified subtropical anticyclone and the passage of an enhanced upper level ridge-trough pattern, typical of cold surge conditions.

To test the role of the Hoggar mountains in the existence and strength of the Tidihelt jet, a control experiment is compared with a counterfactual experiment in which the Hoggar mountains are smoothed to be continuous with the Saharan sand sheet over the region of the SHL. The two experiments are run in parallel for the period 2004–2007 to overlap with available SEVIRI data and the 30 composite high wind, high dust days are compared. The following results are found when the Hoggar mountains are removed in the composites:

1. Mean composite wind speeds within the Tidihelt region decline from 9.0 to 7.3 m s⁻¹, although a slight local maximum persists over central Algeria
2. The wind regime shifts from favoring northeasterlies to a more easterly prevailing wind
3. The Hoggar mountains are responsible for a geopotential height perturbation at 850 hPa of –15 to –20 m over the TID region, but with significant differences extending as far west as the Atlantic coast
4. The northern limb of this cyclonic circulation is collocated with the Tidihelt jet
5. A dome-shaped daytime elevated heating structure situated over the Hoggar mountains can explain the simulated wind field difference between the experiments, indicating an orographic thermal low is responsible for peak Tidihelt winds
6. Based on an empirical relationship between surface wind speeds and LLJ dust observed in SEVIRI imagery, an absence of Hoggar mountains is estimated to reduce dust emission frequency over the Tidihelt region by an average of 31%

The results of this orography experiment show that the Hoggar mountains play a direct role in the surface wind field of the northern Sahara, including the dusty northeasterly LLJ alley through central Algeria. Elevated diabatic heating is shown to be an effective explanation for accelerated low-level flow around a shallow heat low disturbance centered around the lee of the Hoggar mountains. This, in turn, is estimated to have a substantial role in dust emission frequency in LLJ-dominated regions.

This work contributes to a body of literature demonstrating the role that orography plays in both the erosivity and erodibility of key western Saharan dust sources. However, it is limited in scope to LLJs, which are thought to play a secondary role in summertime dust emission. The availability of convective-permitting simulations (e.g., Heinold et al., 2013; Knippertz et al., 2009; Marsham et al., 2011) and CPO parameterizations (e.g., Grandpeix & Lafore, 2010; Pantillon et al., 2015) means more attention could be devoted to orographic impacts upon

convective triggering and cold pool formation around southern Saharan and Sahelian dust sources. The dust budget from year to year in the Sahara is a function of both the availability of erodible material and the frequency and strength of mesoscale meteorological emission mechanisms. Efforts to understand the controls on these emission mechanisms will allow model estimates of dust emission to be constrained via improvements to driving wind fields.

Data Availability Statement

MSG SEVIRI data are available online from the EUMETSAT Data Centre (<https://navigator.eumetsat.int/product/EO:EUM:DAT:MSG:HRSEVIRI>). ERA5 data is maintained by the European Centre for Medium-Range Weather Forecasts and is available from the Copernicus Climate Change Service (<https://climate.copernicus.eu/climate-reanalysis>). IGRA data can be accessed from the National Centers for Environmental Information at <https://www.ncdc.noaa.gov/data-access/weather-balloon/integrated-global-radiosonde-archive>.

References

Acknowledgments

T. Caton Harrison is funded through the NERC doctoral training partnership (NE/L002612/1) and by a CASE studentship with the UK Met Office. R. Washington was partly supported by the NERC-Department for International Development (DFID)-funded Improving Model Processes for African Climate (IMPALA) project (Grant NE/M017206/1), as part of the Future Climate for Africa (FCFA) program (<http://futureclimateafrica.org/project/impala/>). The authors are grateful to Callum Munday, Ian Ashpole and Ron Miller for useful discussions about experiment design and interpretation of the results. The authors would also like to thank three anonymous reviewers for their comments which improved the manuscript.

- Ackerman, S. A. (1997). Remote sensing aerosols using satellite infrared observations. *Journal of Geophysical Research: Atmospheres*, 102(D14), 17069–17079. <https://doi.org/10.1029/96jd03066>
- Allen, C. J., & Washington, R. (2014). The low-level jet dust emission mechanism in the central sahara: Observations from Bordj-Badji Mokhtar during the June 2011 Fennec intensive observation period. *Journal of Geophysical Research: Atmospheres*, 119(6), 2990–3015. <https://doi.org/10.1002/2013jd020594>
- Allen, C. J., Washington, R., & Engelstaedter, S. (2013). Dust emission and transport mechanisms in the central Sahara: Fennec ground-based observations from Bordj-Badji Mokhtar, June 2011. *Journal of Geophysical Research: Atmospheres*, 118(12), 6212–6232. <https://doi.org/10.1002/jgrd.50534>
- Allen, C. J., Washington, R., & Saci, A. (2015). Dust detection from ground-based observations in the summer global dust maximum: Results from Fennec 2011 and 2012 and implications for modeling and field observations. *Journal of Geophysical Research: Atmospheres*, 120(3), 897–916. <https://doi.org/10.1002/2014jd022655>
- Ashpole, I., & Washington, R. (2012). An automated dust detection using SEVIRI: A multiyear climatology of summertime dustiness in the central and western Sahara. *Journal of Geophysical Research: Atmospheres*, 117(D8). <https://doi.org/10.1029/2011jd016845>
- Ashpole, I., & Washington, R. (2013). A new high-resolution central and western Saharan summertime dust source map from automated satellite dust plume tracking. *Journal of Geophysical Research: Atmospheres*, 118(13), 6981–6995. <https://doi.org/10.1002/jgrd.50554>
- Birch, C. E., Parker, D. J., Marsham, J. H., & Devine, G. M. (2012). The effect of orography and surface albedo on stratification in the summertime Saharan boundary layer: Dynamics and implications for dust transport. *Journal of Geophysical Research: Atmospheres*, 117(D5). <https://doi.org/10.1029/2011jd015965>
- Blackadar, A. (1957). Boundary layer wind maxima and their significance for the growth of nocturnal inversions. *Bulletin of the American Meteorological Society*, 38(5), 283–290. <https://doi.org/10.1175/1520-0477-38.5.283>
- Boucher, O., Randall, D., Artaxo, P., Bretherton, C., Feingold, G., Forster, P., et al. (2013). Clouds and aerosols. In *Climate change 2013: The physical science basis. Contribution of Working Group I to the Fifth Assessment Report of the Intergovernmental Panel on Climate Change* (pp. 571–657). Cambridge University Press.
- Brindley, H., Knippertz, P., Ryder, C., & Ashpole, I. (2012). A critical evaluation of the ability of the spinning enhanced visible and infrared imager (SEVIRI) thermal infrared red-green-blue rendering to identify dust events: Theoretical analysis. *Journal of Geophysical Research: Atmospheres*, 117(D7). <https://doi.org/10.1029/2011jd017326>
- Brown, A., Beare, R., Edwards, J., Lock, A., Keogh, S., Milton, S., & Walters, D. (2008). Upgrades to the boundary-layer scheme in the met office numerical weather prediction model. *Boundary-Layer Meteorology*, 128(1), 117–132. <https://doi.org/10.1007/s10546-008-9275-0>
- Caton Harrison, T., Washington, R., & Engelstaedter, S. (2019). A 14-year climatology of Saharan dust emission mechanisms inferred from automatically tracked plumes. *Journal of Geophysical Research: Atmospheres*, 124(16), 9665–9690. <https://doi.org/10.1029/2019jd030291>
- Caton Harrison, T., Washington, R., & Engelstaedter, S. (2021). Satellite-derived characteristics of Saharan cold pool outflows during boreal summer. *Journal of Geophysical Research: Atmospheres*, 126(3), e2020JD033387. <https://doi.org/10.1029/2020jd033387>
- Chellali, F., Khellaf, A., Belouchrani, A., & Reციou, A. (2011). A contribution in the actualization of wind map of Algeria. *Renewable and Sustainable Energy Reviews*, 15(2), 993–1002. <https://doi.org/10.1016/j.rser.2010.11.025>
- Cowie, S. M., Knippertz, P., & Marsham, J. (2014). A climatology of dust emission events from northern Africa using long-term surface observations. *Atmospheric Chemistry and Physics*, 14(16), 8579–8597. <https://doi.org/10.5194/acp-14-8579-2014>
- Cowie, S. M., Marsham, J. H., & Knippertz, P. (2015). The importance of rare, high-wind events for dust uplift in northern Africa. *Geophysical Research Letters*, 42(19), 8208–8215. <https://doi.org/10.1002/2015gl065819>
- Dee, D., Uppala, S., Simmons, A., Berrisford, P., Poli, P., Kobayashi, S., et al. (2011). The ERA-Interim reanalysis: Configuration and performance of the data assimilation system. *Quarterly Journal of the Royal Meteorological Society*, 137(656), 553–597. <https://doi.org/10.1002/qj.828>
- De Longueville, F., Hountondji, Y.-C., Henry, S., & Ozer, P. (2010). What do we know about effects of desert dust on air quality and human health in West Africa compared to other regions? *Science of the Total Environment*, 409(1), 1–8. <https://doi.org/10.1016/j.scitotenv.2010.09.025>
- DeMott, P. J., Sassen, K., Poellot, M. R., Baumgardner, D., Rogers, D. C., Brooks, S. D., & Kreidenweis, S. M. (2003). African dust aerosols as atmospheric ice nuclei. *Geophysical Research Letters*, 30(14). <https://doi.org/10.1029/2003gl017410>
- Drobinski, P., Sultan, B., & Janicot, S. (2005). Role of the Hoggar massif in the West African monsoon onset. *Geophysical Research Letters*, 32(1). <https://doi.org/10.1029/2004gl020710>
- Durre, I., Vose, R. S., & Wuerz, D. B. (2006). Overview of the integrated global radiosonde archive. *Journal of Climate*, 19(1), 53–68. <https://doi.org/10.1175/jcli3594.1>
- Engelstaedter, S., Tegen, I., & Washington, R. (2006). North African dust emissions and transport. *Earth-Science Reviews*, 79(1), 73–100. <https://doi.org/10.1016/j.earscirev.2006.06.004>

- Engelstaedter, S., Washington, R., Flamant, C., Parker, D. J., Allen, C., & Todd, M. (2015). The Saharan heat low and moisture transport pathways in the central Sahara—Multi-aircraft observations and Africa-LAM evaluation. *Journal of Geophysical Research: Atmospheres*, *120*(10), 4417–4442. <https://doi.org/10.1002/2015jd023123>
- Evan, A. T., Fiedler, S., Zhao, C., Menut, L., Schepanski, K., Flamant, C., & Doherty, O. (2015). Derivation of an observation-based map of North African dust emission. *Aeolian Research*, *16*, 153–162. <https://doi.org/10.1016/j.aeolia.2015.01.001>
- Fiedler, S., Knippertz, P., Woodward, S., Martin, G. M., Bellouin, N., Ross, A. N., et al. (2016). A process-based evaluation of dust-emitting winds in the CMIP5 simulation of HadGEM2-ES. *Climate Dynamics*, *46*(3–4), 1107–1130. <https://doi.org/10.1007/s00382-015-2635-9>
- Fiedler, S., Schepanski, K., Heinold, B., Knippertz, P., & Tegen, I. (2013). Climatology of nocturnal low-level jets over North Africa and implications for modeling mineral dust emission. *Journal of Geophysical Research: Atmospheres*, *118*(12), 6100–6121. <https://doi.org/10.1002/jgrd.50394>
- Flamant, C., Chaboureaud, J.-P., Parker, D., Taylor, C., Cammas, J.-P., Bock, O., et al. (2007). Airborne observations of the impact of a convective system on the planetary boundary layer thermodynamics and aerosol distribution in the inter-tropical discontinuity region of the West African monsoon. *Quarterly Journal of the Royal Meteorological Society*, *133*(626), 1175–1189. <https://doi.org/10.1002/qj.97>
- García-Carreras, L., Marsham, J., Parker, D., Bain, C., Milton, S., Saci, A., et al. (2013). The impact of convective cold pool outflows on model biases in the Sahara. *Geophysical Research Letters*, *40*(8), 1647–1652. <https://doi.org/10.1002/grl.50239>
- Grandpeix, J. Y., & Lafore, J.-P. (2010). A density current parameterization coupled with Emanuel's convection scheme. Part I: The models. *Journal of the Atmospheric Sciences*, *67*(4), 881–897. <https://doi.org/10.1175/2009jas3044.1>
- Gregory, D., & Rowntree, P. (1990). A mass flux convection scheme with representation of cloud ensemble characteristics and stability-dependent closure. *Monthly Weather Review*, *118*(7), 1483–1506. [https://doi.org/10.1175/1520-0493\(1990\)118<1483:amfcsv>2.0.co;2](https://doi.org/10.1175/1520-0493(1990)118<1483:amfcsv>2.0.co;2)
- Heinold, B., Knippertz, P., & Beare, R. J. (2015). Idealized large-eddy simulations of nocturnal low-level jets over subtropical desert regions and implications for dust-generating winds. *Quarterly Journal of the Royal Meteorological Society*, *141*(690), 1740–1752. <https://doi.org/10.1002/qj.2475>
- Heinold, B., Knippertz, P., Marsham, J., Fiedler, S., Dixon, N., Schepanski, K., et al. (2013). The role of deep convection and nocturnal low-level jets for dust emission in summertime West Africa: Estimates from convection-permitting simulations. *Journal of Geophysical Research: Atmospheres*, *118*(10), 4385–4400. <https://doi.org/10.1002/jgrd.50402>
- Hoose, C., Lohmann, U., Erdin, R., & Tegen, I. (2008). The global influence of dust mineralogical composition on heterogeneous ice nucleation in mixed-phase clouds. *Environmental Research Letters*, *3*(2), 025003. <https://doi.org/10.1088/1748-9326/3/2/025003>
- Huneeus, N., Schulz, M., Balkanski, Y., Griesfeller, J., Prospero, M., Kinne, S., et al. (2011). Global dust model intercomparison in AeroCom phase I. *Atmospheric Chemistry and Physics*, *11*(15), 7781–7816. <https://doi.org/10.5194/acp-11-7781-2011>
- Jickells, T., An, Z., Andersen, K. K., Baker, A., Bergametti, G., Brooks, N., et al. (2005). Global iron connections between desert dust, ocean biogeochemistry, and climate. *Science*, *308*(5718), 67–71. <https://doi.org/10.1126/science.1105959>
- Kalu, A. (1979). The African dust plume: Its characteristics and propagation across West Africa in winter. *Saharan Dust*, 95–118.
- Klein, H., Nickovic, S., Haunold, W., Bundke, U., Nillius, B., Ebert, M., et al. (2010). Saharan dust and ice nuclei over central Europe. *Atmospheric Chemistry and Physics*, *10*(21), 10211–10221. <https://doi.org/10.5194/acp-10-10211-2010>
- Knippertz, P., Deutscher, C., Kandler, K., Müller, T., Schulz, O., & Schütz, L. (2007). Dust mobilization due to density currents in the atlas region: Observations from the Saharan mineral dust experiment 2006 field campaign. *Journal of Geophysical Research: Atmospheres*, *112*(D21). <https://doi.org/10.1029/2007jd008774>
- Knippertz, P., Trentmann, J., & Seifert, A. (2009). High-resolution simulations of convective cold pools over the northwestern Sahara. *Journal of Geophysical Research: Atmospheres*, *114*(D8). <https://doi.org/10.1029/2008jd011271>
- Kok, J. F., Adebisi, A. A., Albani, S., Balkanski, Y., Checa-García, R., Chin, M., et al. (2021). Contribution of the world's main dust source regions to the global cycle of desert dust. *Atmospheric Chemistry and Physics*, *21*(10), 8169–8193. <https://doi.org/10.5194/acp-21-8169-2021>
- Lavaysse, C., Flamant, C., Janicot, S., Parker, D. J., Lafore, J.-P., Sultan, B., & Pelon, J. (2009). Seasonal evolution of the West African heat low: A climatological perspective. *Climate Dynamics*, *33*(2–3), 313–330. <https://doi.org/10.1007/s00382-009-0553-4>
- Lensky, I., & Rosenfeld, D. (2008). Clouds-aerosols-precipitation satellite analysis tool (CAPSAT). *Atmospheric Chemistry and Physics*, *8*(22), 6739–6753. <https://doi.org/10.5194/acp-8-6739-2008>
- Lock, A., Brown, A., Bush, M., Martin, G., & Smith, R. (2000). A new boundary layer mixing scheme. Part I: Scheme description and single-column model tests. *Monthly Weather Review*, *128*(9), 3187–3199. [https://doi.org/10.1175/1520-0493\(2000\)128<3187:anblms>2.0.co;2](https://doi.org/10.1175/1520-0493(2000)128<3187:anblms>2.0.co;2)
- Lott, F., & Miller, M. J. (1997). A new subgrid-scale orographic drag parameterization: Its formulation and testing. *Quarterly Journal of the Royal Meteorological Society*, *123*(537), 101–127. <https://doi.org/10.1002/qj.49712353704>
- Luo, C., Mahowald, N. M., & Del Corral, J. (2003). Sensitivity study of meteorological parameters on mineral aerosol mobilization, transport, and distribution. *Journal of Geophysical Research: Atmospheres*, *108*(D15). <https://doi.org/10.1029/2003jd003483>
- Mahowald, N. M., Kloster, S., Engelstaedter, S., Moore, J. K., Mukhopadhyay, S., McConnell, J. R., et al. (2010). Observed 20th century desert dust variability: Impact on climate and biogeochemistry. *Atmospheric Chemistry and Physics*, *10*(22), 10875–10893. <https://doi.org/10.5194/acp-10-10875-2010>
- Marsham, J. H., Hobby, M., Allen, C., Banks, J., Bart, M., Brooks, B., et al. (2013). Meteorology and dust in the central Sahara: Observations from fennec supersite-1 during the June 2011 intensive observation period. *Journal of Geophysical Research: Atmospheres*, *118*(10), 4069–4089. <https://doi.org/10.1002/jgrd.50211>
- Marsham, J. H., Knippertz, P., Dixon, N. S., Parker, D. J., & Lister, G. (2011). The importance of the representation of deep convection for modeled dust-generating winds over West Africa during summer. *Geophysical Research Letters*, *38*(16). <https://doi.org/10.1029/2011gl048368>
- Martcorena, B., & Bergametti, G. (1995). Modeling the atmospheric dust cycle: 1. Design of a soil-derived dust emission scheme. *Journal of Geophysical Research: Atmospheres*, *100*(D8), 16415–16430. <https://doi.org/10.1029/95jd00690>
- Messaoudi, D., Setrou, N., Negrou, B., Rahmouni, S., Setrou, B., & Mayou, I. (2019). Site selection methodology for the wind-powered hydrogen refueling station based on AHP-GIS in Adrar, Algeria. *Energy Procedia*, *162*, 67–76. <https://doi.org/10.1016/j.egypro.2019.04.008>
- Middleton, N., & Goudie, A. (2001). Saharan dust: Sources and trajectories. *Transactions of the Institute of British Geographers*, *26*(2), 165–181. <https://doi.org/10.1111/1475-5661.00013>
- Miller, R., Perlwitz, J., & Tegen, I. (2004). Feedback upon dust emission by dust radiative forcing through the planetary boundary layer. *Journal of Geophysical Research: Atmospheres*, *109*(D24). <https://doi.org/10.1029/2004jd004912>
- Miller, R., & Tegen, I. (1998). Climate response to soil dust aerosols. *Journal of Climate*, *11*(12), 3247–3267. [https://doi.org/10.1175/1520-0442\(1998\)011<3247:crtsda>2.0.co;2](https://doi.org/10.1175/1520-0442(1998)011<3247:crtsda>2.0.co;2)
- Murphy, J., Harris, G., Sexton, D., Kendon, E., Bett, P., Clark, R., et al. (2018). *UKCP18 land projections: Science report*.
- Pantillon, F., Knippertz, P., Marsham, J. H., & Birch, C. E. (2015). A parameterization of convective dust storms for models with mass-flux convection schemes. *Journal of the Atmospheric Sciences*, *72*(6), 2545–2561. <https://doi.org/10.1175/jas-d-14-0341.1>

- Parker, D., Burton, R., Diongue-Niang, A., Ellis, R., Felton, M., Taylor, C., et al. (2005). The diurnal cycle of the west African monsoon circulation. *Quarterly Journal of the Royal Meteorological Society*, 131(611), 2839–2860. <https://doi.org/10.1256/qj.04.52>
- Pérez, C., Nickovic, S., Pejanovic, G., Baldasano, J. M., & Özsoy, E. (2006). Interactive dust-radiation modeling: A step to improve weather forecasts. *Journal of Geophysical Research: Atmospheres*, 111(D16). <https://doi.org/10.1029/2005jd006717>
- Pokharel, A. K., & Kaplan, M. L. (2019). Organization of dust storms and synoptic-scale transport of dust by kelvin waves. *Earth System Dynamics*, 10(4), 651–666. <https://doi.org/10.5194/esd-10-651-2019>
- Price, H., Baustian, K., McQuaid, J., Blyth, A., Bower, K., Choulaton, T., et al. (2018). Atmospheric ice-nucleating particles in the dusty tropical Atlantic. *Journal of Geophysical Research: Atmospheres*, 123(4), 2175–2193. <https://doi.org/10.1002/2017jd027560>
- Prospero, J. M., Ginoux, P., Torres, O., Nicholson, S. E., & Gill, T. E. (2002). Environmental characterization of global sources of atmospheric soil dust identified with the nimbus 7 total ozone mapping spectrometer (toms) absorbing aerosol product. *Reviews of Geophysics*, 40(1). <https://doi.org/10.1029/2000rg000095>
- Rác, Z., & Smith, R. K. (1999). The dynamics of heat lows. *Quarterly Journal of the Royal Meteorological Society*, 125(553), 225–252. <https://doi.org/10.1002/qj.4971255313>
- Ramon, J., Lledó, L., Torralba, V., Soret, A., & Doblas-Reyes, F. J. (2019). What global reanalysis best represents near-surface winds? *Quarterly Journal of the Royal Meteorological Society*, 145(724), 3236–3251. <https://doi.org/10.1002/qj.3616>
- Redl, R., Fink, A. H., & Knippertz, P. (2015). An objective detection method for convective cold pool events and its application to northern Africa. *Monthly Weather Review*, 143(12), 5055–5072. <https://doi.org/10.1175/mwr-d-15-0223.1>
- Reynolds, R. W., Rayner, N. A., Smith, T. M., Stokes, D. C., & Wang, W. (2002). An improved in situ and satellite sst analysis for climate. *Journal of Climate*, 15(13), 1609–1625. [https://doi.org/10.1175/1520-0442\(2002\)015<1609:aiais>2.0.co;2](https://doi.org/10.1175/1520-0442(2002)015<1609:aiais>2.0.co;2)
- Ridley, D., Heald, C., & Ford, B. (2012). North African dust export and deposition: A satellite and model perspective. *Journal of Geophysical Research: Atmospheres*, 117(D2). <https://doi.org/10.1029/2011jd016794>
- Roberts, A. J., & Knippertz, P. (2014). The formation of a large summertime Saharan dust plume: Convective and synoptic-scale analysis. *Journal of Geophysical Research: Atmospheres*, 119(4), 1766–1785. <https://doi.org/10.1002/2013jd020667>
- Roberts, A. J., Marsham, J. H., & Knippertz, P. (2015). Disagreements in low-level moisture between (re) analyses over summertime West Africa. *Monthly Weather Review*, 143(4), 1193–1211. <https://doi.org/10.1175/mwr-d-14-00218.1>
- Roberts, A. J., Marsham, J. H., Knippertz, P., Parker, D. J., Bart, M., Garcia-Carreras, L., et al. (2017). New Saharan wind observations reveal substantial biases in analysed dust-generating winds. *Atmospheric Science Letters*, 18(9), 366–372. <https://doi.org/10.1002/asl.1765>
- Rodríguez, S., Cuevas, E., Prospero, J., Alastuey, A., Querol, X., López-Solano, J., et al. (2015). Modulation of Saharan dust export by the North African dipole. *Atmospheric Chemistry and Physics*, 15(13), 7471–7486. <https://doi.org/10.5194/acp-15-7471-2015>
- Schepanski, K., Knippertz, P., Fiedler, S., Timouk, F., & Demarty, J. (2015). The sensitivity of nocturnal low-level jets and near-surface winds over the Sahel to model resolution, initial conditions and boundary-layer set-up. *Quarterly Journal of the Royal Meteorological Society*, 141(689), 1442–1456. <https://doi.org/10.1002/qj.2453>
- Schepanski, K., Tegen, I., Laurent, B., Heinold, B., & Macke, A. (2007). A new Saharan dust source activation frequency map derived from MSG-SEVIRI IR-channels. *Geophysical Research Letters*, 34(18). <https://doi.org/10.1029/2007gl030168>
- Schepanski, K., Tegen, I., & Macke, A. (2012). Comparison of satellite based observations of Saharan dust source areas. *Remote Sensing of Environment*, 123, 90–97. <https://doi.org/10.1016/j.rse.2012.03.019>
- Schepanski, K., Tegen, I., Todd, M., Heinold, B., Bönsch, G., Laurent, B., & Macke, A. (2009). Meteorological processes forcing Saharan dust emission inferred from MSG-SEVIRI observations of subdaily dust source activation and numerical models. *Journal of Geophysical Research: Atmospheres*, 114(D10). <https://doi.org/10.1029/2008jd010325>
- Schulz, M., Prospero, J. M., Baker, A. R., Dentener, F., Ickes, L., Liss, P. S., et al. (2012). Atmospheric transport and deposition of mineral dust to the ocean: Implications for research needs. *Environmental Science & Technology*, 46(19), 10390–10404. <https://doi.org/10.1021/es300073u>
- Semazzi, F. H., & Sun, L. (1997). The role of orography in determining the Sahelian climate. *International Journal of Climatology*, 17(6), 581–596. [https://doi.org/10.1002/\(sici\)1097-0088\(199705\)17:6<581::aid-joc134>3.0.co;2-e](https://doi.org/10.1002/(sici)1097-0088(199705)17:6<581::aid-joc134>3.0.co;2-e)
- Smith, R. (1990). A scheme for predicting layer clouds and their water content in a general circulation model. *Quarterly Journal of the Royal Meteorological Society*, 116(492), 435–460. <https://doi.org/10.1002/qj.49711649210>
- Soares, P. M. M., Lima, D. C. A., Semedo, Á., Cardoso, R. M., Cabos, W., & Sein, D. (2019). The north African coastal low level wind jet: A high resolution view. *Climate Dynamics*, 53(1–2), 1211–1230. <https://doi.org/10.1007/s00382-018-4441-7>
- Spengler, T., Reeder, M. J., & Smith, R. K. (2005). The dynamics of heat lows in simple background flows. *Quarterly Journal of the Royal Meteorological Society: A Journal of the Atmospheric Sciences, Applied Meteorology and Physical Oceanography*, 131(612), 3147–3165. <https://doi.org/10.1256/qj.04.177>
- Spengler, T., & Smith, R. K. (2008). The dynamics of heat lows over flat terrain. *Quarterly Journal of the Royal Meteorological Society: A Journal of the Atmospheric Sciences, Applied Meteorology and Physical Oceanography*, 134(637), 2157–2172. <https://doi.org/10.1002/qj.342>
- Stevens, B., Fiedler, S., Kinne, S., Peters, K., Rast, S., Müsse, J., et al. (2017). MACv2-SP: A parameterization of anthropogenic aerosol optical properties and an associated Twomey effect for use in CMIP6. *Geoscientific Model Development*, 10, 433–452. <https://doi.org/10.5194/gmd-10-433-2017>
- Strong, J. D., Vecchi, G. A., & Ginoux, P. (2018). The climatological effect of Saharan dust on global tropical cyclones in a fully coupled GCM. *Journal of Geophysical Research: Atmospheres*, 123(10), 5538–5559. <https://doi.org/10.1029/2017jd027808>
- Todd, M. C., & Cavazos-Guerra, C. (2016). Dust aerosol emission over the Sahara during summertime from cloud-aerosol lidar with orthogonal polarization (CALIOP) observations. *Atmospheric Environment*, 128, 147–157. <https://doi.org/10.1016/j.atmosenv.2015.12.037>
- Todd, M. C., Washington, R., Raghavan, S., Lizcano, G., & Knippertz, P. (2008). Regional model simulations of the Bodélé low-level jet of northern Chad during the Bodélé Dust Experiment (BoDEX 2005). *Journal of Climate*, 21(5), 995–1012. <https://doi.org/10.1175/2007jcli1766.1>
- Vizy, E. K., & Cook, K. H. (2009). A mechanism for African monsoon breaks: Mediterranean cold air surges. *Journal of Geophysical Research: Atmospheres*, 114(D1). <https://doi.org/10.1029/2008jd010654>
- Walters, D., Baran, A. J., Boutle, I., Brooks, M., Earnshaw, P., Edwards, J., et al. (2019). The Met Office Unified Model Global Atmosphere 7.0/7.1 and JULES Global Land 7.0 configurations. *Geoscientific Model Development*, 12(5), 1909–1963. <https://doi.org/10.5194/gmd-12-1909-2019>
- Walters, D., Brooks, M., Boutle, I., Melvin, T., Stratton, R., Vosper, S., et al. (2017). The Met Office Unified Model Global Atmosphere 6.0/6.1 and JULES Global Land 6.0/6.1 configurations. *Geoscientific Model Development*, 10(4), 1487–1520. <https://doi.org/10.5194/gmd-10-1487-2017>
- Washington, R., Flamant, C., Parker, D., Marsham, J., McQuaid, J., Brindley, H., et al. (2012). Fennec—the saharan climate system. *CLIVAR Exchanges*, 17(3), 31–33.
- Washington, R., & Todd, M. C. (2005). Atmospheric controls on mineral dust emission from the bodélé depression, chad: The role of the low level jet. *Geophysical Research Letters*, 32(17). <https://doi.org/10.1029/2005gl023597>

- Washington, R., Todd, M. C., Engelstaedter, S., Mbainayel, S., & Mitchell, F. (2006). Dust and the low-level circulation over the Bodélé Depression, Chad: Observations from BODEX 2005. *Journal of Geophysical Research: Atmospheres*, *111*(D3). <https://doi.org/10.1029/2005jd006502>
- Weaver, C. J., Joiner, J., & Ginoux, P. (2003). Mineral aerosol contamination of tiros operational vertical sounder (TOVS) temperature and moisture retrievals. *Journal of Geophysical Research: Atmospheres*, *108*(D8). <https://doi.org/10.1029/2002jd002571>
- Wolyn, P. G., & Mckee, T. B. (1994). The mountain-plains circulation east of a 2-km-high north-south barrier. *Monthly Weather Review*, *122*(7), 1490–1508. [https://doi.org/10.1175/1520-0493\(1994\)122<1490:tmpeco>2.0.co;2](https://doi.org/10.1175/1520-0493(1994)122<1490:tmpeco>2.0.co;2)
- Wu, C., Lin, Z., & Liu, X. (2020). The global dust cycle and uncertainty in CMIP5 (coupled model intercomparison project phase 5) models. *Atmospheric Chemistry and Physics*, *20*(17), 10401–10425. <https://doi.org/10.5194/acp-20-10401-2020>
- Zängl, G., & Chico, S. G. (2006). The thermal circulation of a grand plateau: Sensitivity to the height, width, and shape of the plateau. *Monthly Weather Review*, *134*(9), 2581–2600. <https://doi.org/10.1175/mwr3207.1>